# COUPLING AN ICE SHEET MODEL TO EC-EARTH

Jeroen van Lent

19 January 2013

*Supervisors*

Roderik van de Wal

Richard Bintanja

Bas de Boer

UTRECHT UNIVERSITY

INSTITUTE FOR MARINE AND ATMOSPHERIC RESEARCH UTRECHT (IMAU)

ROYAL NETHERLANDS METEOROLOGICAL INSTITUTE (KNMI)

# COUPLING AN ICE SHEET MODEL TO EC-EARTH

## ABSTRACT

The evolution of ice sheets is determined by climate and the climate is affected by the presence of the ice sheet. For climate models, this means that a coupling of ice sheets and climate is needed in order to understand both. However, the difference in time scales in which both evolve poses a difficulty for coupling the two. Ice sheets have a response time of millenia, while climate models typically assess climate problems on a much shorter scale. Usually, this issue is solved by prescribing the ice sheets in climate models, but on intermediate timescales it is not a priori obvious whether ice sheet coupling can be neglected.

In this project, a one-way coupling from the ESM EC-Earth to the GRICE Greenland ice sheet model is achieved. As surface mass balance (SMB) is not available as output from EC-Earth data, a method of calculating the SMB from available EC-Earth output data is presented. Here, the temperature and precipitation fields from EC-Earth, which were obtained from a historic run (1850-2000) and the RCP4.5 radiative forcing scenario (2000-2100) are used to force the SMB over the period 1850-2100. For a past-glacial climate forcing required to spin-up the model, a global temperature record was used as a perturbation.

SMB is calculated by separating between accumulation and run-off, using EC-Earth data for accumulation and parameterizing the run-off as a height-dependent perturbation of a reference field, using a modification of the SMB gradient method from Helsen et al. (2012). A climate perturbation is introduced by modifying the surface height with temperature. Following this method, a reconstruction of present-day climate is presented, as well as projections for the evolution of the Greenland ice sheet in the 21st century. The model predicts a best estimate for global sea-level rise of 79 mm, with a range between 61 and 105 mm. This is within the range of 0-17 cm found by Graversen et al. (2011).

**Acknowledgments**

First of all, I would like to thank Bas de Boer for his invaluable help and advice that helped me tremendously in finishing this project. I'd also like to extend my profound gratitude to Roderik van de Wal and Richard Bintanja for their assistance and supervision. Furthermore, I'd like to thank Michiel Helsen for his useful contributions, mainly in developing an SMB parameterization able to work with EC-Earth, and Michael Kliphuis for his technical assistance and teaching me about the GRICE model. I'd also like to thank the people at the MK department of the KNMI for providing me with a work place. Finally, I'd like to thank my parents and my brother for their support during this project.

**Table of Contents**

# Chapter 1
# Introduction

## 1.1 Ice sheets

Ice sheets are massive bodies of ice, spanning entire continents. The Earth has currently only two of these: the largest one on Antarctica and a smaller one on Greenland. Approximately 77% of the world's fresh water supply is currently locked within the two major ice sheets on the planet, namely the Antarctic ice sheet (AIS), and the Greenland ice sheet (GrIS) (figure 1). The GrIS alone holds enough water to raise global sea level with 7 m if it were to be released into the oceans. The AIS holds far more even, enough for over 60 m of sea level rise.

The presence of the ice sheets influences global climate because of their albedo (surface reflectivity). Since they are year-round covered by highly reflective snow, the ice sheets naturally reflect most incoming radiation, 'cooling off' the planet. Loss of ice sheet surface area would decrease the planetary albedo and more radiation would get absorbed instead, warming the Earth's surface.

## 1.2 Importance of ice sheet modeling

In recent years, research in climate change has become increasingly important, especially where future climate change predictions are concerned. The IPCC Assessment Report (AR4) has, with use of computer models, predicted a substantial increase in global temperature mostly due to increased anthropogenic greenhouse gases like $CO_2$. Coupled with this are a number of other predicted changes in global and local climate, such as precipitation changes. Sea level rise is also predicted, due to increased melting of the ice sheets on Antarctica and Greenland.

A lot of climate change predictions come from Global Climate Models (GCMs), which are advanced computer models that simulate climate behaviour on a global scale. Most of the current state-of-the-art GCMs that are being used for this task are Atmosphere-Ocean General Circulation Models (AOGCMs), which are coupled circulation models that compute the general circulation of the earth's atmosphere and ocean, as well as their interaction.

In order to make more accurate predictions, however, various subsystems which also affect global climate should also be taken into account, which are currently neglected or prescribed, such as ocean biochemistry, carbon cycle components and dynamic ice sheets. Models which take these subsystems and their interaction with


Figure 1: Geographic map of Greenland, including the ice sheet with ice thickness over 10 m above bedrock or sea level. Image by Eric Gaba, 2011. Licensed under Creative Commons Attribution-Share Alike 3.0 Unported license.

one another into account can be referred to as Earth System Models (ESMs).

One such ESM currently in development is EC-Earth, which is based on the European Centre for Medium-range Weather Forecast (ECMWF) weather prediction model. Currently, it operates as a high-end AOGCM, but is being expanded into a full ESM, a process in which the global climate division of the KNMI has taken the lead. Incorporating ice sheet dynamics into this model is a vital step towards achieving this goal.

### 1.3 Coupling ice sheet models to GCMs

Over the course of history, global climate has known dramatic shifts and changes. Ice sheets react to these changes by expanding or retracting in response to changes in temperature and precipitation. However, because of their size, they tend to be slow to react to rapid changes. They evolve on a different timescale than the climate. While atmospheric and oceanic conditions may change on the order of decades, ice sheets typically evolve on a timescale of millennia. As a result, an ice sheet holds a memory of past climate. This means that the Greenland ice sheet we observe today has not yet fully adjusted from the Last Glacial Maximum (LGM), the period of maximum ice extent, about 20,000 years ago. The warm, current climate has not yet permeated through the core of the ice sheet, therefore the temperatures deep within the ice sheet are observed to be colder than one would expect if the ice sheet had fully adjusted to present-day temperatures.

In ice sheet modeling, this slow adjustment is important to consider. In order to find an accurate representation of the currently observed ice sheets, an ice sheet model should be allowed to evolve for over thousands of years, using past climate data as input. This is usually referred to as spin-up time, which will be discussed in greater detail in section 3.3.

Here also lies the crux with incorporating ice sheet models with global climate models. Since global climate models typically simulate several decades up to a few centuries of climate evolution, while ice sheet models need to be run for millennia in order to be accurate, ice sheet models cannot readily be incorporated into a climate model.

Most of the time, the climate models just prescribe the ice sheets, using offline calculations of ice sheet volume based on the temperature scenarios from these GCMs.

neglecting ice sheet evolution altogether. Ice volume changes are calculated offline by an ice sheet model

On short timescales, this abstraction is fine. On intermediate timescales of centuries, however, the effects of ice sheets cannot a priori be neglected. The evolution

of climate will have a profound effect on the ice sheet, and likewise will the changes within the ice sheet have its own feedbacks on the climate itself (ie. changes in albedo and surface height). It is therefore of importance to achieve a coupling of ice sheet models and global climate models and take these effects into account.

### 1.4 Purpose of this project

This project concerns the research towards a coupling of the GRICE Greenland Ice-sheet model with the Earth System Model EC-Earth. For this, two goals have been defined:

1. Achieve improved projections of the mass budget of the Greenland ice sheet over the course of the 21st century by using EC-Earth output data.
2. Startup of one-way coupling the GRICE model to EC-Earth to benefit goal #1. A one-way coupling of EC-Earth to GRICE should be achieved.

### 1.5 Chapter outline

In Chapter 2, the basics of the GRICE model will be discussed. The focus of this chapter will be the mass balance scheme used to calculate the evolution of the ice sheet. Ice dynamics will only be briefly touched upon, as they were not the focus of this research. In Chapter 3, the setup of the model will be explained in greater detail. Specifically, the parameters and reference fields used are mentioned, as well as the climate forcing used to calculate ice sheet evolution for the spin-up sequence. Furthermore, the incorporation of EC-Earth data into the model with which present-day reconstructions and future predictions of the Greenland ice sheet can be found will be discussed. The results of the model will be shown in Chapter 4, starting with model tuning to present-day climate. This will be followed by reconstructions of present-day climate, and finally model predictions for SMB, total mass flux and sea-level rise for the 21st century. Conclusions will be drawn in Chapter 5, also incorporating a discussion on the model performance and an outlook on future research.

# Chapter 2
# Model description

In this chapter, the GRICE ice-sheet model, which was used for this research, will be discussed. The focus of this chapter lies in the mass balance parameterization scheme that was used in the model. The calculation of ice dynamics within the model will only briefly be touched upon, as they were not the focus of this research.

## 2.1 The GRICE ice sheet model

GRICE is a 3-D thermomechanical ice sheet model, developed by the Institute of Marine and Atmospheric research Utrecht (IMAU). It is based on the ANICE model (e.g. van de Wal, 1999a,b; Helsen et al., 2012), which has been applied for several other studies (e.g. Bintanja and van de Wal, 2008; Graversen et al., 2010; de Boer et al., 2012). GRICE is in principle identical to the ANICE model, but its use is exclusively for the Greenland ice sheet (GrIS). Both models are based upon the same approximations and use the same calculation methods to calculate the ice dynamics. The purpose behind the development of GRICE as a separate model is to provide a suitable ice sheet model for the GrIS that can be coupled with EC-Earth (see section 1.4).

## 2.2 Ice dynamics

The dynamics of an ice sheet depend on several properties: ice thickness, surface slope and ice temperature within the ice sheet. Ice temperature depends on the geothermal heat flux at the base of the ice sheet, heat generation by deformation of ice and by friction between the ice and the underlying bedrock, and the air temperature at the surface.

Thermomechanical ice sheet models relate ice flow and temperature through the temperature dependent flow parameter $K(T)$ of the ice. In the GRICE model, this parameter arises in Glen's flow law:

$$\dot{\epsilon}_{ij} = K(T)\tau_e^{n-1}\tau_{ij}, \tag{1}$$

which relates the strain rate $\dot{\epsilon}_{ij}$, to the ice stresses $\tau$. The value of the exponent $n$ needs to be experimentally determined. For Greenland, this value is taken to be 3.

Furthermore, the ice dynamics are calculated based on the shallow ice approximation (SIA, Hutter, 1983), which is a widely used approximation in ice sheet

modeling. Essentially, it means that ice sheets are mainly deformed by the basal shear stress, which is a solid approximation for large ice sheets as the Greenland ice sheet. Since the stiffness of the ice depends on its temperature, thermodynamics are included to take this into account. The ice temperature is calculated based on the 3-D advection, diffusion, friction, the geothermal heat flux ($G$) at the bottom, as well as the annual surface temperature $T_s$, adjusted for the effects of refreezing (see section 2.6).

At points near the bed where the temperature and pressure causes the ice to reach its melting point, the ice is allowed to slide over the bed. For this, a Weertman type sliding law is used (Weertman, 1964), corrected for the effect of sub-glacial water pressure (Bindschadler, 1983). The forming of ice shelves is not allowed in the model. When the ice approaches the grounding line, it breaks off. Explicit calving physics and shelf dynamics are not included (see also section 2.7).

### 2.3 The surface mass balance

The behaviour of ice sheets is, like many other processes involving global climate, far too complex to describe in detail. Certain assumptions and parameterizations are needed to simplify an ice sheet model to a workable degree. The performance of an ice sheet model therefore can greatly depend on the choice of parameters and the level of detail it is able to resolve.

One of the most crucial parts of such parameterized calculations to the ice sheet model performance is how its surface mass balance (SMB) is calculated. Usually, SMB at a particular grid point at time $t$ is defined as:

$$\mathrm{SMB}(t) = A(t) - R(t), \tag{2}$$

with $A(t)$ representing accumulation due to precipitation (snowfall), and $R(t)$ representing melt, or run-off. This quantity therefore represents the net effect of the surface sources and sinks.

SMB forces the ice flow: the simulated ice sheet responds to a change in the mass balance, which is why a correct calculation is of such importance. Unfortunately, the processes associated with SMB, accumulation and run-off due to melt, are complex variables and cannot readily be calculated. Most GCMs, like EC-Earth, do not provide SMB as output, but only provide fields for temperature and precipitation. From these two fields, SMB needs to be reconstructed.

Accumulation is derived from precipitation, which is entirely dependent on weather patterns and can therefore vary with every year. Though present-day accumulation is reasonably well constrained by measurements, records of precipitation

data are obviously absent for thousands of years in the past. While accumulation follows from the precipitation field provided by EC-Earth in a relatively simple way (section 2.4), ablation (run-off) does not. Melt is a function of the components of the surface energy balance, which can vary both spatially and temporally to a high degree. Melt-water percolates through the glacier before it ends up as run-off, changing the local ice dynamics. Part of it is also not drained instantly, but surface melt-water refreezes again in the colder interior before it is removed. This makes it a difficult process to model, and has to be treated separately from accumulation when coupling an ice sheet model to a GCM. Finding a suitable parameterization to deal with this problem is often the challenge in modeling ice sheets. In the following sections, a strategy for coupling EC-Earth data to the SMB will be presented.

### 2.4 Calculation of the accumulation

EC-Earth provides monthly output of both a 2 meter temperature ($T(t)$) and precipitation ($P(t)$) field, both of which are used to perturb the SMB. To do so, the SMB needs to be separated into accumulation and ablation, using equation 2, and calculating both separately.

These fields, however, are only available for the period 1850-2100. For the past-glacial period up to 1850, the model cannot be directly forced by EC-Earth data. A different solution for this period has to be used, which should connect with EC-Earth data at the year 1850. To ensure that the model progresses smoothly from one period to another, the $T_{1850}$ and $P_{1850}$ fields (figures 2a and 2b) are used as reference values. During the past-glacial period, a $\Delta T$ record is introduced as a perturbation of the $T_{1850}$ field, so that

$$T_{\mathrm{pg}}(t) = T_{1850} + \Delta T(t) - \Gamma_{\mathrm{atm}} \Delta H_s(t) \tag{3}$$

where $T_{\mathrm{pg}}(t)$ is the temperature field during the period before 1850, corrected for surface height changes $\Delta H_s(t) = H_s(t) - H_{s,\mathrm{ref}}$ using a constant atmospheric lapse rate of $\Gamma_{\mathrm{atm}} = 7.3743$ K km$^{-1}$. Note that $\Delta T$ is a scalar value and therefore has no spatial variations. It is a global temperature offset over the entire domain. Section 3.3 provides further explanation regarding this period. At 1850, the value for $\Delta T$ becomes 0, so that $T_{\mathrm{pg}}(t = 1850) = T_{1850}$ and thus at this point direct forcing from EC-Earth data can commence.

The precipitation field from EC-Earth needs to be adjusted for these temperature differences during the past-glacial period in order to be able to perturb the accumulation with temperature. To do so, the reference temperature, $T_{1850}$, as well as the current temperature $T_{\mathrm{pg}}(t)$ first have to be adjusted for the free atmospheric

temperature $T_{\mathrm{inv}}(t)$ (method of Jouzel and Merlivat, 1984):

$$\begin{aligned} T_{\mathrm{inv}}(t) =& 88.9 + 0.67 * T_{\mathrm{pg}}(t) \\ T_{\mathrm{inv,1850}} =& 88.9 + 0.67 * T_{1850} \end{aligned} \tag{4}$$

Next, the fraction of the precipitation that falls as snow ($f_s(t)$) needs to be determined (following Ohmura et al., 1999):

$$f_s(t) = 0.5 * (1 - \frac{\arctan{(\frac{T_{\mathrm{pg}}(t) - T_0}{3.5})}}{1.25664}), \tag{5}$$

with $T_0$ the triple point of water, 273.16 K. As $f_s(t)$ is a fraction, its value is constrained between 0 and 1. It should be noted that the fraction that falls as rain is not used by the model. The accumulation, $A_{\mathrm{pg}}$, can then be calculated as follows:

$$A_{\mathrm{pg}}(t) = P_{1850} \times 1.04^{(T_{\mathrm{inv}}(t) - T_{\mathrm{inv,1850}})} \times f_s(t), \tag{6}$$

where $P_{1850}$ is the precipitation field for the year 1850.

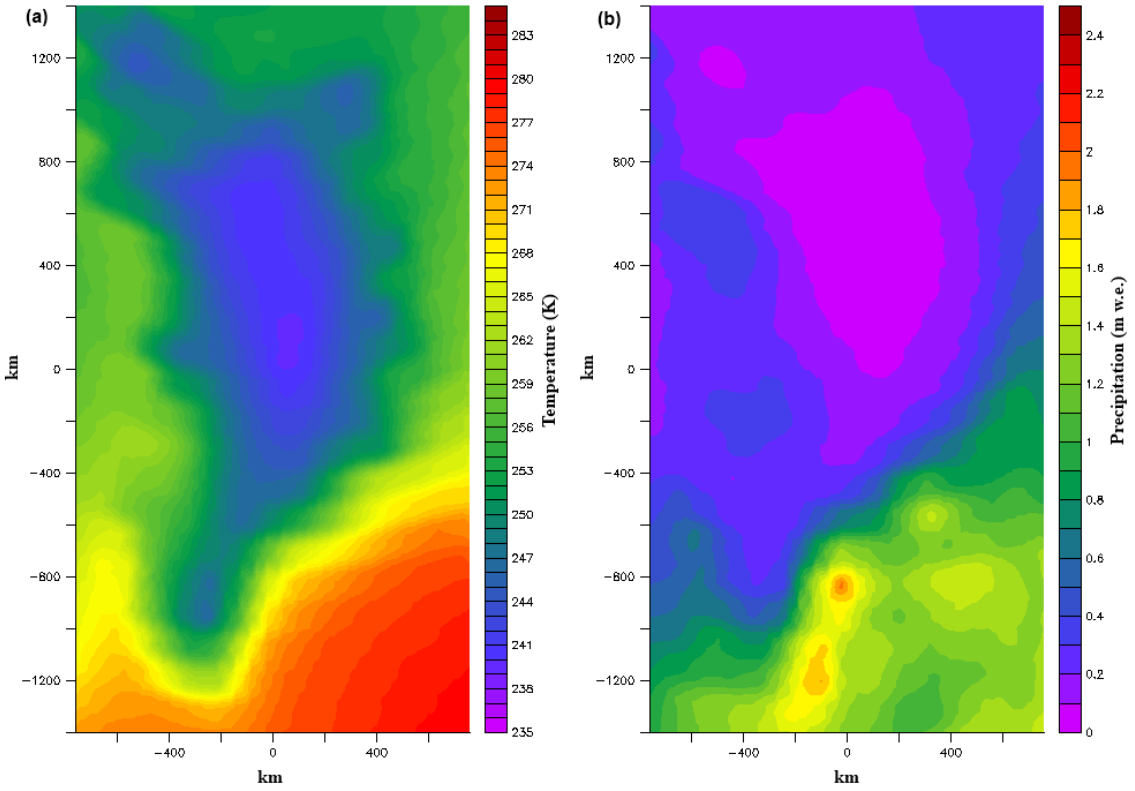


Figure 2: EC-Earth 1850 reference fields. a) Annual mean of the 1850 temperature field (in Kelvin). b) Total yearly precipitation for 1850 (in m w.e.).

For the period $1850 \leq t \leq 2100$, the same method can be used, though here the monthly varying EC-Earth temperature $T(t)$ can be used directly. $\Delta T(t)$ is zero during this period, and thus $T(t)$ only needs to be adjusted for elevation changes:

$$T_{\Delta H_s}(t) = T(t) - \Gamma_{\text{atm}} \Delta H_s(t) \tag{7}$$

The precipitation field can be corrected following equation 4, substituting $T_{\text{pg}}(t)$ and $T_{1850}$ with the corrected $T_{\Delta H_s}(t)$ and the uncorrected $T(t)$, respectively. Equation 5 then becomes

$$f_s(t) = 0.5 * (1 - \frac{\arctan{(\frac{T_{\Delta H_s}(t) - T_0}{3.5})}}{1.25664}) \tag{8}$$

and the accumulation $A(t)$ (equation 6):

$$A(t) = P(t) \times 1.04^{(T_{\text{inv},\Delta H_s}(t) - T_{\text{inv}}(t))} \times f_s(t), \tag{9}$$

where $P(t)$ is the monthly precipitation field from EC-Earth.

### 2.5 Calculation of the ablation

#### 2.5.1 PDD method

There are several methods generally used to provide a workable calculation of the ablation. One of these is a Positive Degree-Days (PDD) method. This method calculates ablation by using a statistical relationship between temperatures above melting point and melt rates of snow and ice. The performance of such a model relies on the correct choice of a number of parameters. While still widely used (Graversen et al., 2011), this method has the drawback of being only dependent on the surface temperature and not, for example, changes in solar insolation or surface height. Consequently, use of a PDD method may lead to an overestimation of the climate sensitivity (Helsen et al., 2012).

#### 2.5.2 Regional $H_s$-SMB relation

A completely different method of parameterizing the SMB was recently proposed by Helsen et al. (2012), which directly adjusts SMB to changes in surface elevation ($H_s(t)$) and/or climate forcing. This is achieved by the use of a regional $H_s$-SMB relation: a lapse rate corrects the local SMB due to changes in $H_s(t)$ according to the following equation:

$$\text{SMB}(t) = a + bH_s(t), \tag{10}$$

where $a$ and $b$ are spatially varying, but time-constant coefficients that need to be determined. To do so, Helsen et al. (2012) separates the accumulation (SMB $> 0$) and ablation (SMB $< 0$) regimes, and selects at least 100 pairs of surface height and SMB from each regime in a search radius of 150 km or more for a reference climate. In this case, the reference surface height, $H_{s,\mathrm{ref}}$, is obtained from the mapping by Bamber et al. (2003, figure 3b) and reference SMB, $\mathrm{SMB}_{\mathrm{ref}}$, from the 1958-2007 average result of the regional climate model RACMO2/GR (Ettema et al., 2009), which provides a realistic result of the present day GrIS SMB (figure 4a). For each regime, a simple linear regression line through the data points provides the coefficients $a$ and $b$, as shown in figure 5, with the additional constraint that the regression line is forced through its reference value. This process creates a different relation for each regime, and thus at a time $t$, SMB is determined as

$$\mathrm{SMB(t)} = \begin{cases} a_{\mathrm{acc}} + b_{\mathrm{acc}} H_s(t) & \text{if } H_s > H_c \\ a_{\mathrm{abl}} + b_{\mathrm{abl}} H_s(t) & \text{if } H_s < H_c \end{cases} \tag{11}$$

$H_c$ can be considered a critical surface height. It is calculated as the surface elevation where the regression lines of both regimes intersect. $H_s(t)$ is the time-dependent surface elevation. If the The coefficients $a_{\mathrm{acc}}$, $b_{\mathrm{acc}}$, $a_{\mathrm{abl}}$ and $b_{\mathrm{abl}}$ are determined over the entire domain and are shown in figure 6.

To prevent positive values of $b_{\mathrm{acc}}$ from enforcing a positive feedback between $H_s$ and SMB when $H_s$ is perturbed, the value for SMB needs to be maximized. Negative values for the same parameter may also lead to problems, because when $H_s$ increases, the SMB can eventually become negative in the accumulation regime. Helsen et al. (2012) uses the following conditions at every grid point to keep SMB within reasonable limits in the accumulation regime:

$$\mathrm{SMB}_{\mathrm{max}} = \max(\overline{\mathrm{SMB}_{\mathrm{pos}}}, \mathrm{SMB}_{\mathrm{ref}}) \tag{12}$$

$$\mathrm{SMB}_{\mathrm{min}} = \begin{cases} 0.25 \times \overline{\mathrm{SMB}_{\mathrm{pos}}} & \text{if } \mathrm{SMB}_{\mathrm{ref}} < 0 \\ 0.25 \times \mathrm{SMB}_{\mathrm{ref}} & \text{if } \mathrm{SMB}_{\mathrm{ref}} > 0 \end{cases} \tag{13}$$

where $\overline{\mathrm{SMB}_{\mathrm{pos}}}$ refers to the mean positive SMB value within the search area.

This mass balance scheme can be perturbed by climate scenarios by modifying the surface height at a particular time according to

$$H_{s,\Delta T}(t) = H_s(t) + \frac{\Delta T(t)}{\Gamma_{\mathrm{atm}}}, \tag{14}$$

with $\Delta T(t)$ the climate perturbation (the deviation from a reference temperature at

time $t$) and $\Gamma_{\text{atm}}$ the atmospheric lapserate. An increase in temperature will therefore relate to a lower $H_{s,\Delta T}$, and thus a lower SMB. The rate of decrease depends on the regime, as well as the location on the ice sheet, as the SMB gradients vary spatially. $H_{s,\Delta T}(t)$ then replaces $H_s(t)$ in equation 11.

### 2.5.3 EC-Earth coupling method

While the method described above provides an acceptable calculation of SMB, difficulties arise when input from GCMs (in this case EC-Earth) is introduced. While Helsen et al. (2012) provides a manner of adjusting SMB to a climate perturbation, the only field that can be used is temperature. Precipitation is another variable that needs to be included, and this method offers no ready solution, as it does not calculate accumulation and ablation separately, but only the net SMB. It is therefore unable to respond to climate perturbations in precipitation. Since only a method for calculating ablation is needed, the method from Helsen et al. (2012) needs to be modified so that ablation is obtained instead of the net SMB. Finding a suitable parameterization for the ablation, while retaining the $H_s$-SMB gradient method was one of the focus points of this project.

As only run-off needs to be calculated, the coefficients given by Helsen et al. (2012) cannot readily be used, as they are calculated using the net SMB, without distinguishing between accumulation and run-off. While this method does distinguish accumulation and ablation regions, these still only apply to the net SMB, and therefore even in the ablation region, the points used to determine the coefficients are a compound of accumulation and run-off.

To solve this problem, only the gradient in the ablation region is used, as it is assumed that a linear relation exists between the surface height $H_s$ and the run-off $R$. Changes in surface height or temperature therefore perturb the run-off, causing it to increase to a decreasing surface height or temperature, and likewise, decrease to an increase in $H_{s,\Delta T}$. This means that in the ablation region, defined as the region where $H_{s,\Delta T}(t) < H_c$, a run-off perturbation, $\Delta R(t)$ is calculated as

$$\Delta R(t) = \beta(H_{s,\Delta T}(t) - H_{s,\text{ref}})b_{\text{abl}}, \tag{15}$$

with $H_{s,\text{ref}}$ the reference surface height (figure 3b), and $\beta$ a tunable scaling parameter included to account for differences in the gradient $b_{\text{abl}}$ when it is used to only calculate the run-off as opposed to the net SMB. A suitable value for $\beta$ needs to be found through experimental verification. The larger the choice for $\beta$, the larger the contribution of changes in surface height to the total runoff will become. See section 4.3 for further details regarding the determination of a suitable value for $\beta$.

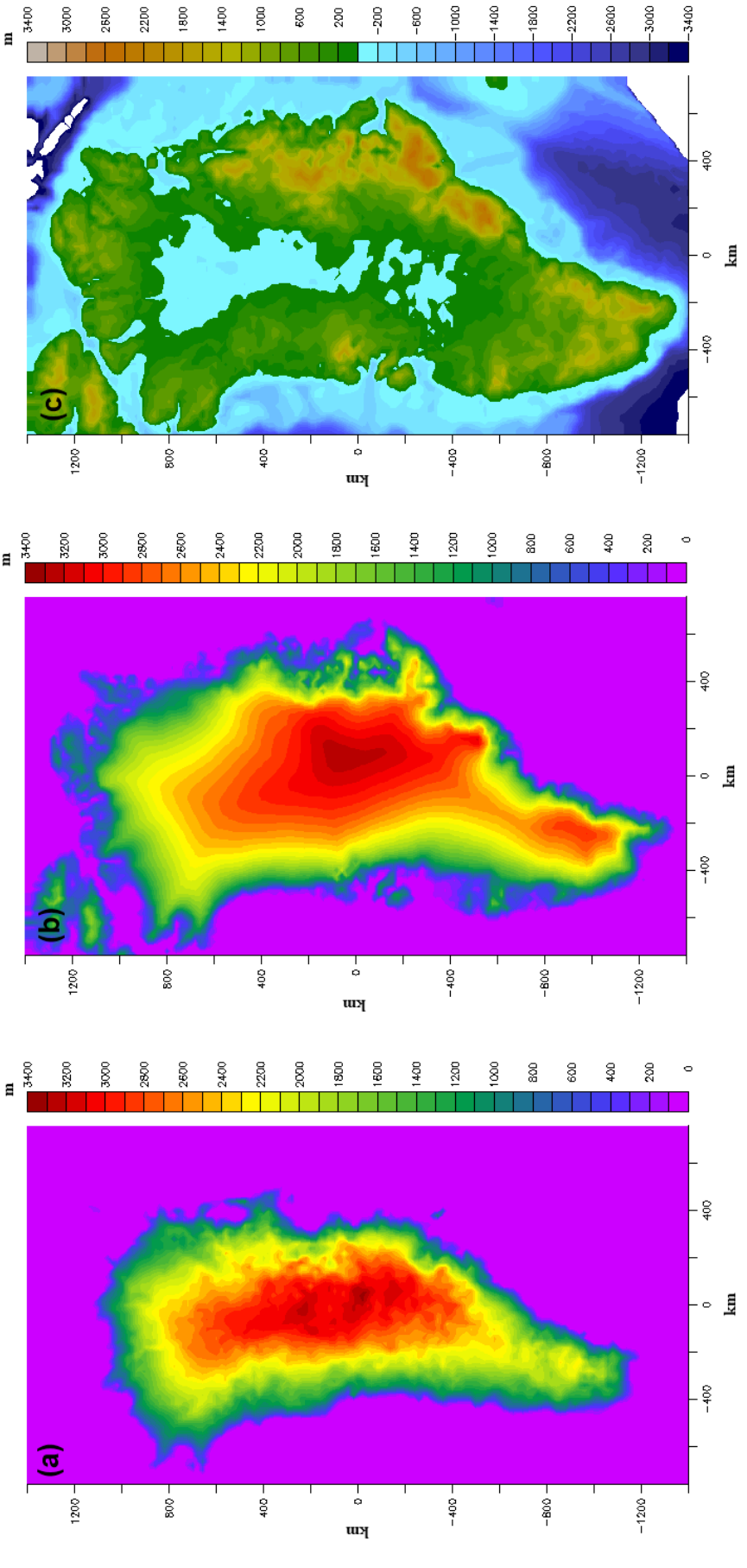


Figure 3: Reference fields for **(a)** ice sheet thickness, **(b)** surface height and **(c)** bedrock elevation. The images were created using the data from Bamber et al. (2003).

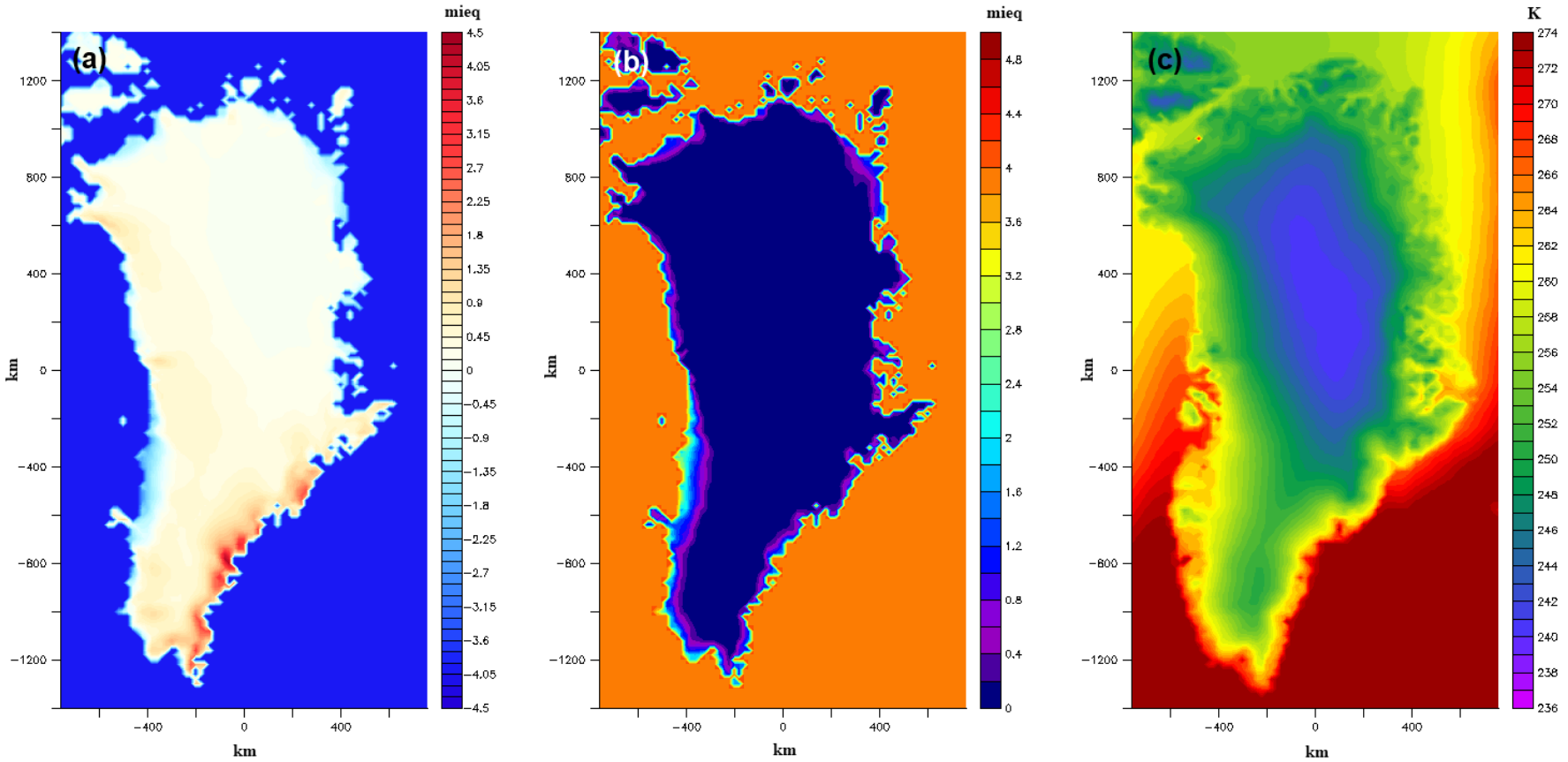


Figure 4: Reference fields for **(a)** SMB, **(b)** run-off and **(c)** ice surface temperature. Run-off was obtained by subtracting accumulation from the SMB field. The images were created using the 1958-2007 average results from the RACMO2/GR regional climate model (Ettema et al., 2009).

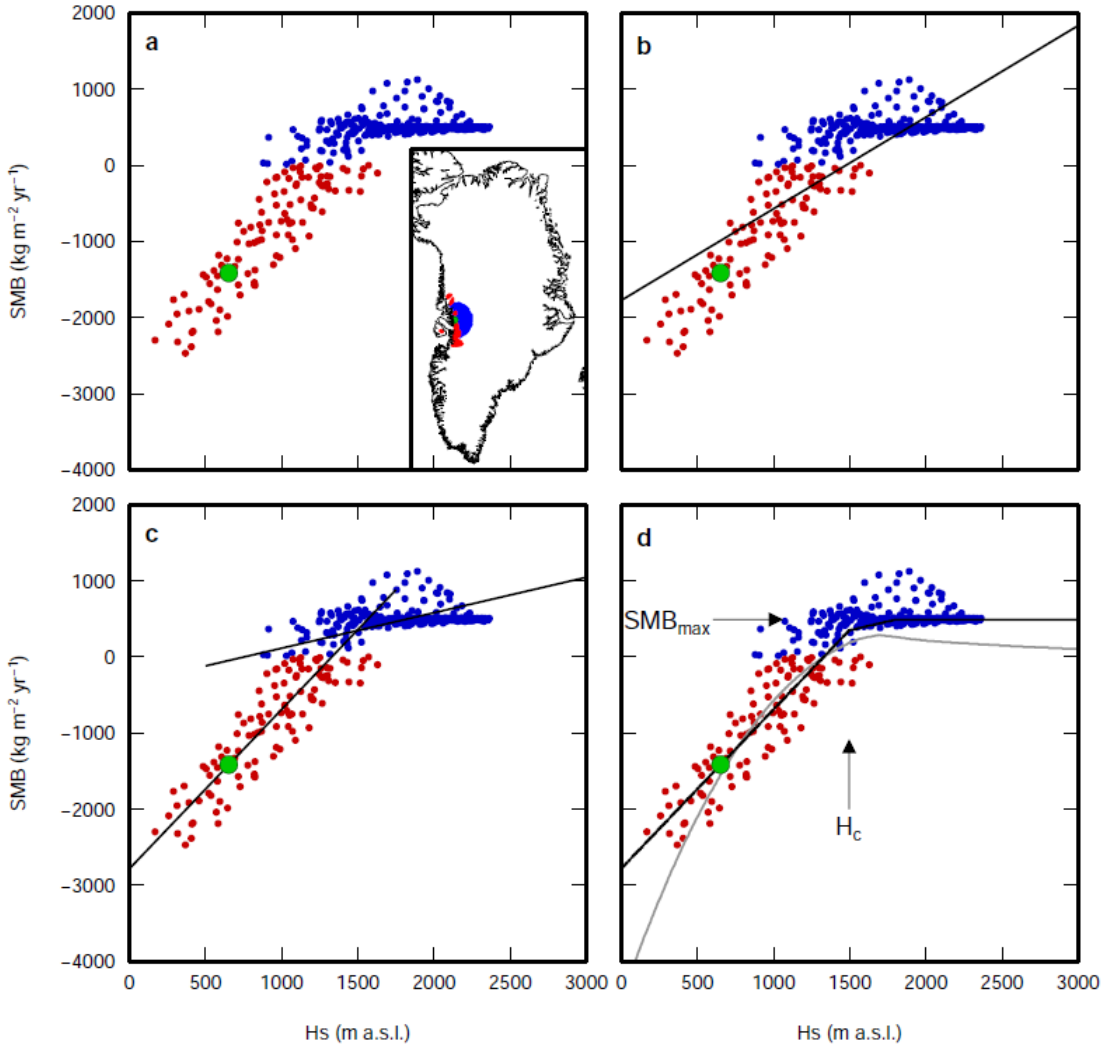


Figure 5: Example for the determination of the $H_s$-SMB coefficients for a point in the ablation zone. The red dots indicate points with a negative SMB, while blue dots represent positive SMB. The green dot marks the reference value for the SMB at this particular location. The black lines denote the regression line fit between $H_s$ and SMB following different methods: **(a)** scatter plot of SMB as a function of $H_s$, inlay shows the location of the data points; **(b)** the gradient line using a simple linear regression fit over all points; **(c)** different linear regression lines for both regimes; **(d)** connected regression lines, maximized to the value $\mathrm{SMB_{max}}$ in the accumulation regime. $H_c$ is shown as the surface height at which the two regression lines connect. The grey line represents SMB calculated by a PDD model. Figure from Helsen et al. (2012).

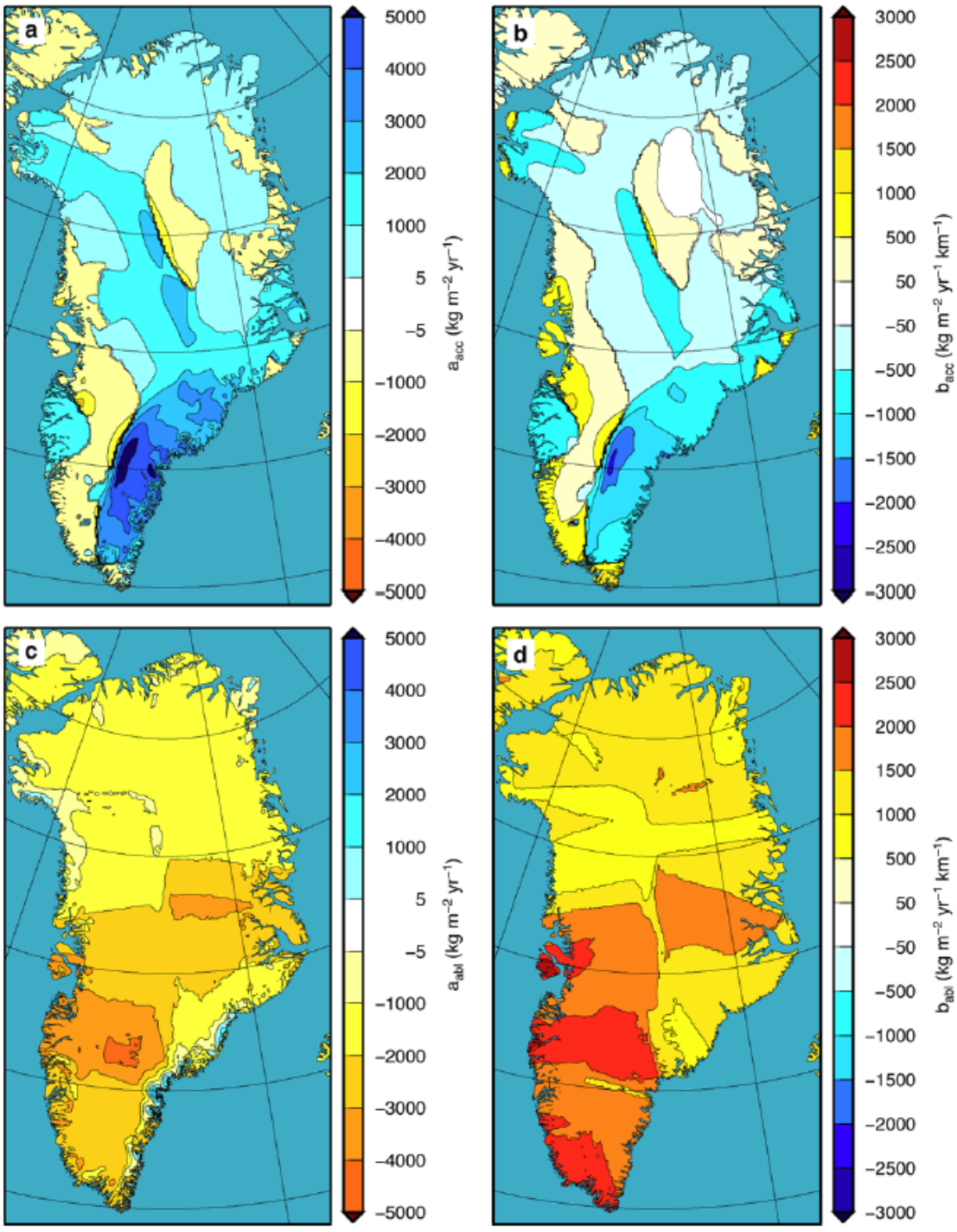


Figure 6: Spatially varying coefficients $a$ and $b$ in equation 11 for the accumulation regime (**(a)** and **(b)**) and the ablation regime (**(c)** and **(d)**).

In the accumulation region ($H_{\Delta T}(t) > H_c$), run-off is assumed to be either small or completely absent, so that $\Delta R$ is always taken to be zero. The total run-off, $R$, is then given by:

$$R(t) = \begin{cases} R_{\text{ref}} & \text{if } H_{s,\Delta T}(t) > H_c \\ R_{\text{ref}} - \Delta R(t) & \text{if } H_{s,\Delta T}(t) < H_c \end{cases}. \tag{16}$$

The reference state $R_{\text{ref}}$ is the 1958-2007 averaged run-off field from the RACMO2/GR regional climate model, shown in figure 4b, which is the run-off component of the SMB field used by Helsen et al. (2012) to determine the $H_s$-SMB coefficients. $R$ is not allowed to become negative, as run-off is taken as a positive quantity. In all cases where $R$ would become negative, its value is set to zero.

The total SMB is calculated using equation 2, with the added constraint that in the accumulation region, a minimum value of $0.25 \times \text{SMB}_{\text{ref}}$ is used to ensure that the mass balance can never become negative in this region.

### 2.6 Refreezing

As mentioned in section 2.2, refreezing of percolating meltwater influences the ice surface temperature and therefore the ice dynamics. This model parameterizes the thermodynamic effect of refreezing on the ice temperature in the same way as Helsen et al. (2012), namely by correcting the mean annual ice surface temperature $T_s$ for elevation changes using a constant atmospheric lapse rate $\Gamma = 7.3743$ K km$^{-1}$. For $T_s$, the RACMO2/GR 1958-2007 mean surface temperature was used (figure 4c). The surface temperature is then adjusted for refreezing (RFR) following Reeh (1991):

$$\Delta T_{s,\text{RFR}} = 26.6 \times \text{RFR} \tag{17}$$

Values for the $H_s$ dependent RFR field are found following Helsen et al. (2012), using the same coefficients, determined from the RACMO2/GR refreezing field (Ettema et al., 2009).

### 2.7 Dynamical discharge

Ice sheets can also lose mass due to calving of icebergs at the ice sheet front, which is often referred to as dynamical discharge ($D(t)$). The SMB together with this discharge constitutes the total mass balance (MB(t)) of an ice sheet:

$$\text{MB}(t) = \text{SMB}(t) - D(t). \tag{18}$$

This is an important distinction to consider, as it can result in an ice sheet losing mass even though its net SMB is positive. Dynamical discharge is a product of ice dynamics and is therefore a (delayed) response to changes in the SMB. Since this process is not a forcing, it needs to be calculated separately from SMB. This is difficult, as iceberg calving can occur suddenly, locally, and can vary immensely in its intensity, which makes them difficult to predict or even estimate. As they cannot properly be resolved on the scale of the model, explicit calving physics are not included. Formation of ice shelves is not allowed, so once the ice sheet approaches the grounding line and starts to float, the ice immediately breaks off, constituting $D(t)$.

### 2.8 Bedrock adjustment

The bedrock underneath an ice sheet is not a static entity. The enormous amounts of ice above it tend to press down the bedrock. Consequently, a receding amount of ice will lighten the bedrock load, causing it to rise. The timescale of this process is in the order of thousands of years. GRICE also adjusts the bedrock as a response to a changing ice load. For this, and Elastic Lithosphere-Relaxing Astenosphere (ELRA) model is used (Le Meur and Huybrechts, 1996), with a bedrock relaxation time of $\tau = 3000$ yr. The reference bedrock elevation is from Bamber et al. (2003, figure 3c).

# Chapter 3
# Experimental setup

In this chapter, the configuration of the GRICE ice sheet model as it was used to generate the results found in chapter 4 will be discussed. These settings include the initial state of the model, the climate forcing during the glacial spin-up, and the EC-Earth climate forcing (from the year 1850 up to 2100) used to generate present-day and future results. Values for parameters used in the model are presented in table 1.

## 3.1 Model grid and resolution

As mentioned in section 2.1, GRICE is a 3-D ice sheet model, which calculates the ice dynamics based on the three dimensional ice temperature and velocity fields. Its horizontal domain consists of 141 $\times$ 77 grid points, achieving a grid separation and thus a horizontal resolution of 20 km. Vertically, the grid consists of 15 layers, which scale with the ice thickness. The resolution is linear initially, but increases close to the bedrock, as here the gradient in the ice velocity is the highest.

## 3.2 Reference fields

The model needs an initial state of the Greenland ice sheet, which evolves during the run. This initial state consists of present-day reference fields of the ice thickness ($H_i$), surface height ($H_s$), bedrock elevation ($H_b$) surface mass balance (SMB), run-off ($R$), surface ice temperature ($T_s$) and a mask which separates ice sheet, grounding line and ocean points. Reference fields of $H_i$, $H_s$ and $H_b$ were taken from Bamber et al. (2003) and are shown in figures 3a, b, and c, respectively. A 10m thick ice layer was introduced for all grid points on the ice thickness field that were within the ice mask, but where ice thickness data was missing (Helsen et al., 2012). SMB and the run-off component thereof were taken from the 1958-2007 average RACMO2/GR regional climate model (Ettema et al., 2009), as well as the reference $T_s$. These are shown in figures 4a, b, c.

All of these fields were interpolated to the GRICE model grid using the OBLIMAP mapping package developed by Reerink et al. (2010). The oblique stereographic projection was centered at 72° N, 40° W and used a projection angle of $\alpha = 7.5°$. The ice mask is shown in figure 7 and only distinguishes ice sheet, grounding line and ocean points, as forming of ice shelves is not allowed in the model (see section 2.7).

| Parameter | Symbol | Value | Unit |
|---|---|---|---|
| Atmospheric lapse rate | $\Gamma$ | 7.3743 | K km$^{-1}$ |
| Bedrock relaxation time | $\tau$ | 3000 | yr |
| Earth surface ocean area | $a_o$ | $3.62\times10^{14}$ | m$^2$ |
| Flow enhancement | m | 3 | - |
| Geothermal heat flux | $G$ | $5.460\times10^{-2}$ | W m$^{-2}$ |
| Glen's flow law exponent | n | 3 | - |
| Gravitational accelleration | g | 9.81 | m s$^{-2}$ |
| Ice density | $\rho_i$ | 910 | kg m$^3$ |
| Mantle density | $\rho_m$ | 3300 | kg m$^3$ |
| Lith. Flexural rigidity | D | $1\times10^{25}$ | N m |
| Seawater density | $\rho_s$ | 1028 | kg m$^3$ |
| Sliding coefficient | $A_s$ | $1.8\times10^{-10}$ | m$^8$ yr$^{-1}$ N$^{-3}$ |
| Triple point of water | $T_0$ | 273.16 | K |
| Water density | $\rho_w$ | 1000 | kg m$^3$ |

Table 1: Ice sheet model parameter values

### 3.3 Past glacial spin-up sequence

As mentioned in section 1.3, it can take several millenia before an ice sheet is fully adjusted to climate changes because temperature changes only dissipate into the interior very slowly. Therefore, just letting a reference ice sheet evolve from present-day conditions through a climate change scenario will not provide accurate results, as this would assume that the ice sheet has fully adjusted to present-day conditions. So, in order to accurately simulate ice-sheet behaviour, the model should be run through a spin-up sequence, which lasts sufficiently long so that, when applying the climate model forcing, no 'memory' of the initial field remains and the resulting ice sheet can be attributed entirely to past forcing. During present-day conditions, then, the model should give a result that is close to observational reference values.

Incorporating a past climate reconstruction, however, is not a straightforward task. In order to be completely accurate, complete temperature and precipitation records for Greenland would be needed for the entire past glacial period, which is a trivial impossibility. Here, past climate is approximated by taking reference precipitation and temperature fields from EC-Earth data (see section 3.4), and perturb these with a global temperature offset. These temperature records are taken from the GRIP $\delta^{18}$O ice core temperature reconstruction for the period from 105 kyr before present (b.p.) up until the start of the climate forcing, and the Vostok $\delta$D record for the period before that. These records were connected by first converting them to a glacial index and then recreating the temperature profile (Greve, 2005). Records are available every 20 years, tied together using simple linear interpolation. The resulting temperature profile from the start of the run to time $t = 0$, where the forcing from

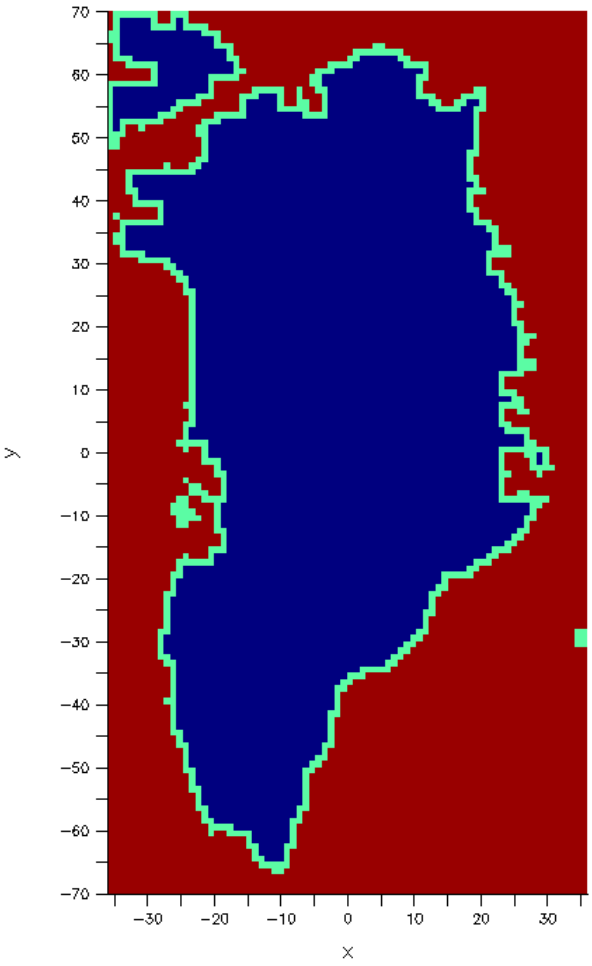


Figure 7: Ice mask used to distinguish ice sheet, grounding line and ocean grid points. The axes show the horizondtal grid numbers. Ice sheet points are shown in blue, ocean points are red and grounding line points are green.

EC-Earth is initiated, is shown in figure 8a. The spin-up sequence is started at 123 kyr b.p., as in this period, global conditions were approximately equal to present-day values.

Past sealevel changes are also incorporated to change surface height elevation accordingly. Here, the Bintanja & van de Wal (2008) reconstruction is used and shown in figure 8b. No sealevel changes are used for the period beyond $t = 0$, as these data were not provided by EC-Earth at this time.

### 3.4 EC-Earth climate forcing

The coupling between EC-Earth and the GRICE ice sheet model is achieved by feeding monthly temperature and precipiation data from EC-Earth output to GRICE. These

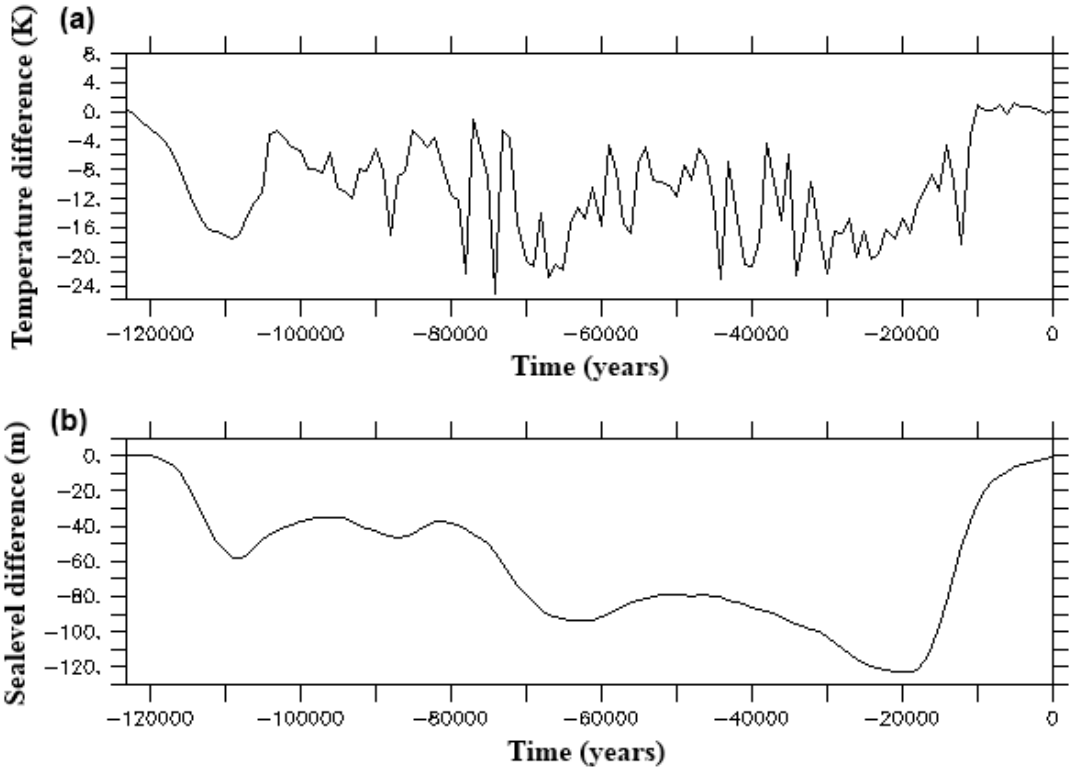


Figure 8: **(a)** Global temperature offset (in Kelvin) from present-day values for the last 123 kyr. **(b)** Sealevel offset (in metres) from present-day values for the last 123 kyr.

fields change the SMB of the ice sheet, and it evolves accordingly (section 2.5.3). The EC-Earth data used for this research are the CMIP5 global climate predictions, adjusted to work for the GRICE model grid. Only the data from 1850 to 2100 are used. From 1850 to 2000, a historic run is used, while for the period 2000-2100, EC-Earth follows the RCP4.5 radiative forcing scenario (figure 9).

After the spin-up cycle described in section 3.3, the monthly forcing from EC-Earth data is initiated at the model time $t = 0$, so that it coincides with the EC-Earth output for the year 1850. The 1850 fields are also used as the reference for the spin-up track (shown in figures 2a and b). The run ends at $t = 250$, which represents the year 2100. During this period, accumulation is calculated with the monthly precipitation and temperature data. Ablation is calculated from this field by modifying $H_s$ following equation 14 at each grid point by the yearly average EC-Earth temperature offset from the 1850 average. The yearly average temperature offset for Greenland, compared to global average values predicted by EC-Earth are shown in figure 10.

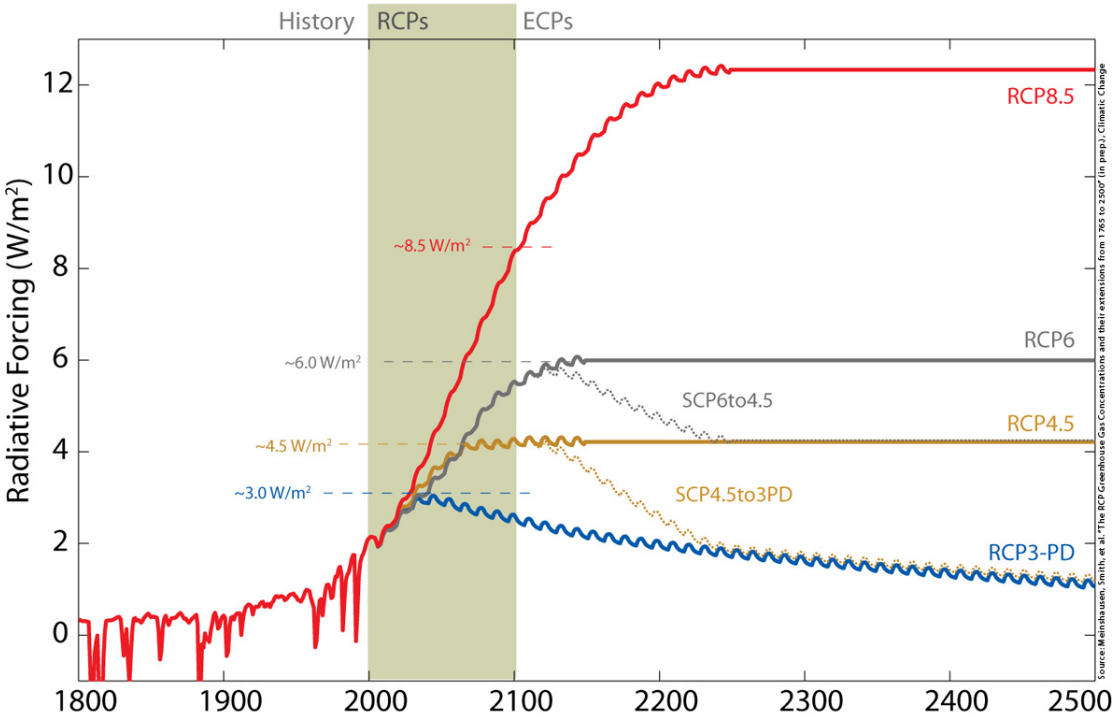


Figure 9: Total radiative forcing for different RCP scenarios. The RCP4.5 scenario used by EC-Earth during 2000-2100 is indicated by the brown line. Figure from Meinshausen et al. (2011).

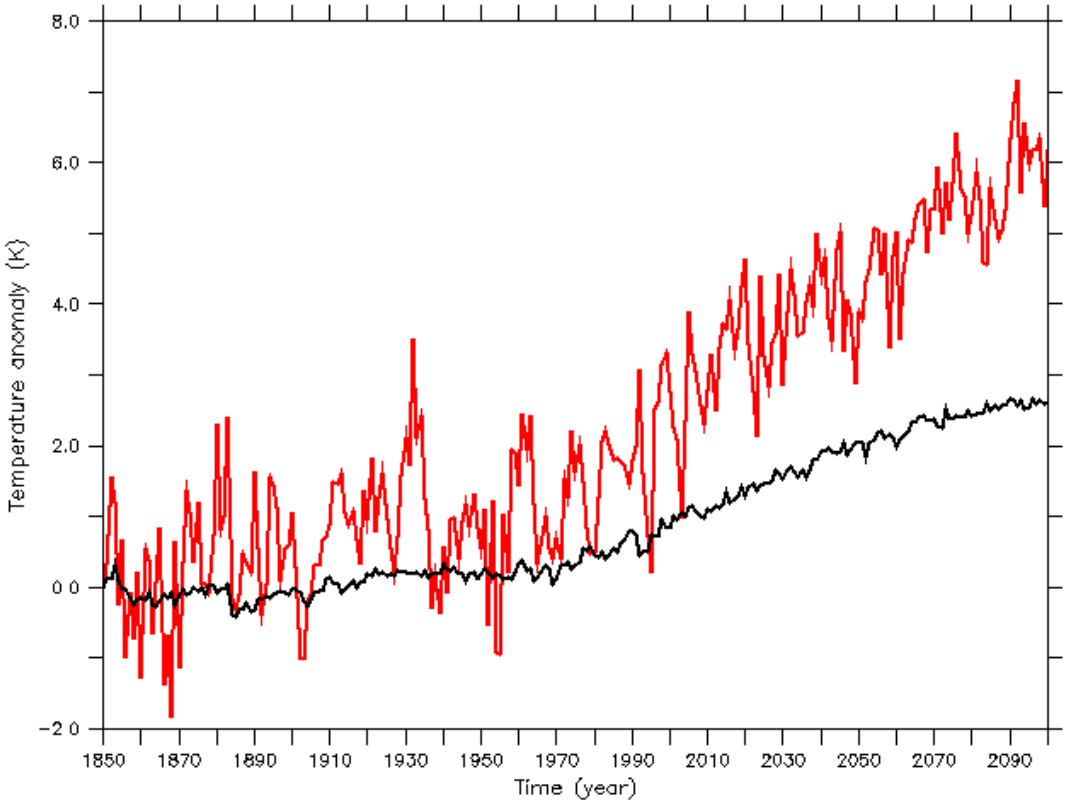


Figure 10: Domain and yearly averaged temperature deviation from 1850 values calculated by EC-Earth for the period 1850-2100. The black line denotes the global average temperature anomaly (1850 value is 285.73 K). The temperature anomalies for Greenland are indicated with the red line (1850 value is 256.39 K). The global $\Delta T(2000-1850)$ is 0.83 K and $\Delta T(2100-2000)$ is 1.78 K. For Greenland, these values are 2.75 K and 3.42 K, respectively. The global mean temperatures from EC-Earth are slightly above the multi-model mean of CMIP5 models for the period 1901-2010 and are near the multi-model mean for the period 2006-2100 (unpublished results, ref. G. Van Oldenborgh, KNMI, personal communication).

# Chapter 4
# Results

In this chapter, the results of the model will be presented. In section 2.5.3, it has been explained that the SMB parameterization used for this research depends upon the tunable parameter $\beta$, which controls the effect of the regional surface height correction to the ablation. As the surface height also depends upon the temperature perturbation, the effect of climate change to the ablation is also influenced by this $\beta$ parameter. It is therefore of vital importance to constrain the value for $\beta$ in such a way that the model provides the best possible agreement with present-day observations. The first few sections of this chapter will deal with this problem, while the latter part will show the model results for the optimal choice for $\beta$. A discussion of these results can be found in chapter 5.

## 4.1 Reference runs

A first step towards finding the correct value for $\beta$, as well as examining the performance of the model is to look at the evolution of the ice sheet with any forcing turned off. For these runs, no temperature or precipitation perturbation is introduced. Only the reference fields of temperature and precipitation are used, which are the EC-Earth monthly fields of 1850. The ice sheet is then allowed to evolve for 20,000 years. By varying the value for $\beta$, an assessment can be made on the stability of the ice sheet.

In figure 11, the results of these reference experiments are displayed. Here, total ice volume over time is shown for different values of $\beta$. The values for the $\beta$-coefficient range from 0.1 up to 1.0. The present-day reference volume of the ice sheet is approximately $2.9 \times 10^{15}$ m$^3$. Initially, the volume of the ice sheet increases for all $\beta$ due to the modeled ice sheet adjusting itself. After 20,000 years, the figure shows that for a value of $\beta$ between 0.1 and 0.5, the ice sheet stabilizes at a total ice volume between $2.7 \times 10^{15}$ m$^3$ and $2.8 \times 10^{15}$ m$^3$. This is slightly lower than the present-day observations, which can possibly be attributed to the use of a pre-industrial historical reconstruction of the temperature and precipitation data of 1850 as opposed to present-day fields, though for run-off, there should be no influence of the temperature field, as only perturbations from this field act towards the climate variability of the run-off. However, the reference run-off field is an averaged field over present-day conditions as opposed to the pre-industrial values used for $T$ and $P$, so the base run-off could be somewhat higher than expected given the input fields, leading to a slightly lower ice volume than expected.

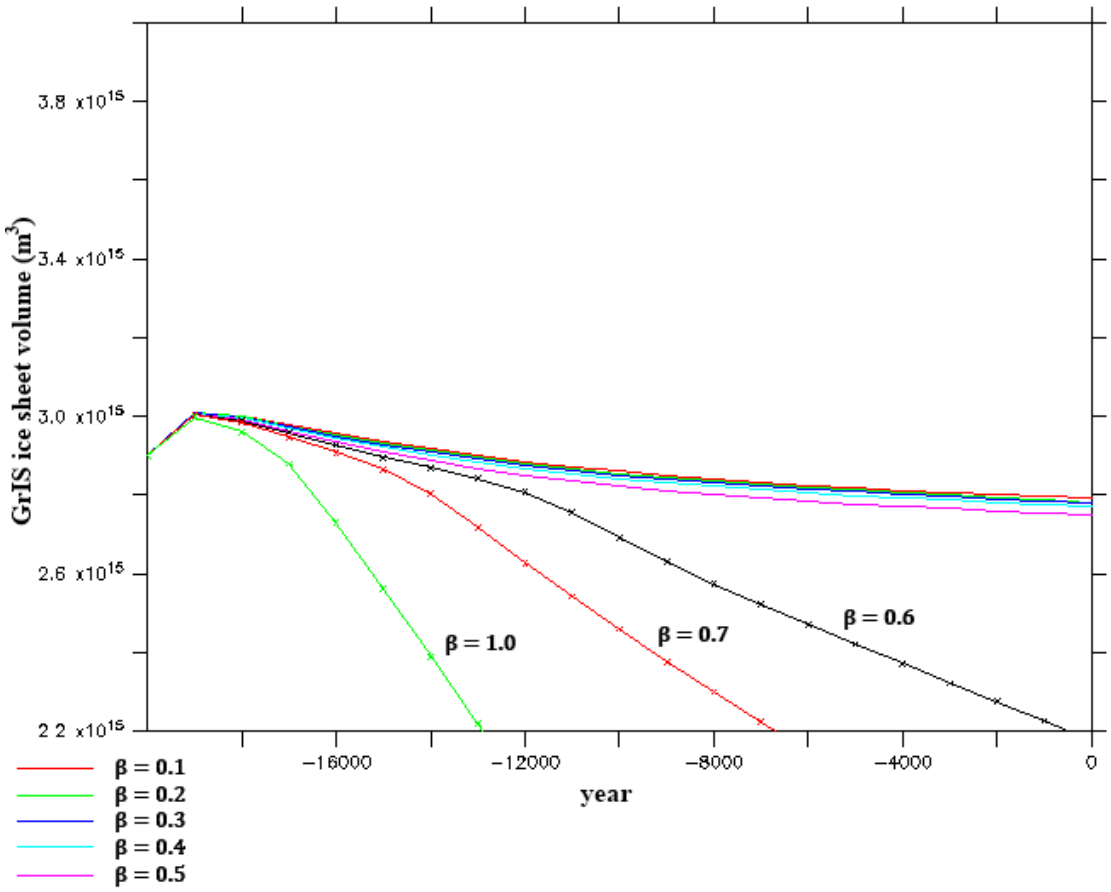


Figure 11: Time evolution of the GrIS ice sheet volume (in $m^3$), using a constant reference forcing from the 1850 monthly temperature and precipitation fields. The colored lines indicate different values of $\beta$, ranging from 0.1 up to 1.0.

As for the different values of $\beta$, from the figure it becomes clear that higher values than $\beta = 0.5$ do not result in a stable ice sheet, even without any climate forcing in play. The ice sheet falls off rapidly, starting in the ablation region in the south-west area of the GrIS, later joined by the northern ablation region. Lower values do result in a stable sheet, so a workable value for $\beta$ needs to be found in this region.

The fact that for a stable ice sheet $\beta$ needs to be much smaller than 1 is likely to be due to the difference in the reference temperature and precipitation fields compared to the RACMO2/GR present-day SMB reconstruction used by Helsen et al. (2012) to force the ice sheet model. The accumulation provided from this field has a higher resolution, which allows local spots of heavier snowfall to be resolved instead of spreading it out over a larger region. Moreover, the low value for $\beta$ can be

attributed to the choice of the single-year 1850 fields, which may have been relatively low in precipitation in that particular year. In order, then, for the ice sheet to become stable, the corresponding ablation has to be downscaled significantly, as the reference run-off field is a present-day situation. This results in a lower value for $\beta$.

### 4.2 Glacial spin-up results

For the glacial spin-up sequence, as mentioned in section 3.3, the runs were started at 123 kyr b.p., as during this period conditions were comparable to those of present-day. From there, the model was forced with the global temperature offset taken from ice core data. Figure 12 shows the results of the entire spin-up track for different values of $\beta$, as well as the results produced following the method of Helsen et al. (2012). This comparison run was started at 123 kyr b.p. as well, using the same temperature offset record. This is different from Helsen et al. (2012), who started their past glacial scenario at the height of the Eemian optimum at 128 kyr b.p. instead, which resulted in lower values for the ice sheet volume compared to the ones shown here.

Here, $\beta$ was varied between intermediate values of 0.25 and 0.45. Values lower than 0.25 did not provide acceptable results, as they clearly underpredicted the effects of temperature change on run-off. A value of $\beta = 0.5$ was also discarded as an acceptable value, as the ice sheet started to vanish during the last 10 kyr of the spin-up track (where the transition into the present interglacial period takes place).

The figure shows agreement between different values of $\beta$ as far as the past glacial period is concerned. This agreement can be attributed to the run-off being minimal or even completely absent during large periods within the spin-up sequence, as temperatures were generally much lower than present-day conditions (see figure 8, hence the volume changes during this period are mainly driven by changes in accumulation. This observation is strengthened by the divergence of the values for $\beta$ after the transition into the present-day interglacial. Here, too, the values of the ice sheet volume at the end of the run are slighly below observational values. Comparing these results to those obtained following the method of Helsen et al. (2012), it follows that the ice sheet seems to adjust to changes in climate somewhat more quickly and more intensely when using the SMB calculation method as presented in this report.

The ice sheet volume during the last glacial maximum (LGM), which occurred at approximately 20 kyr b.p. lies slightly below $3.6 \times 10^{15}$ m$^3$, which is slightly above the peak value found by Helsen et al. (2012) of $3.56 \times 10^{15}$ m$^3$, but still in the lower range of earlier reconstructions and that paleoclimatic evidence would suggest. This may be explained that, similar with the method used by Helsen et al., ice shelf formation is not allowed and so ice shelf physics are not incorporated in the model,

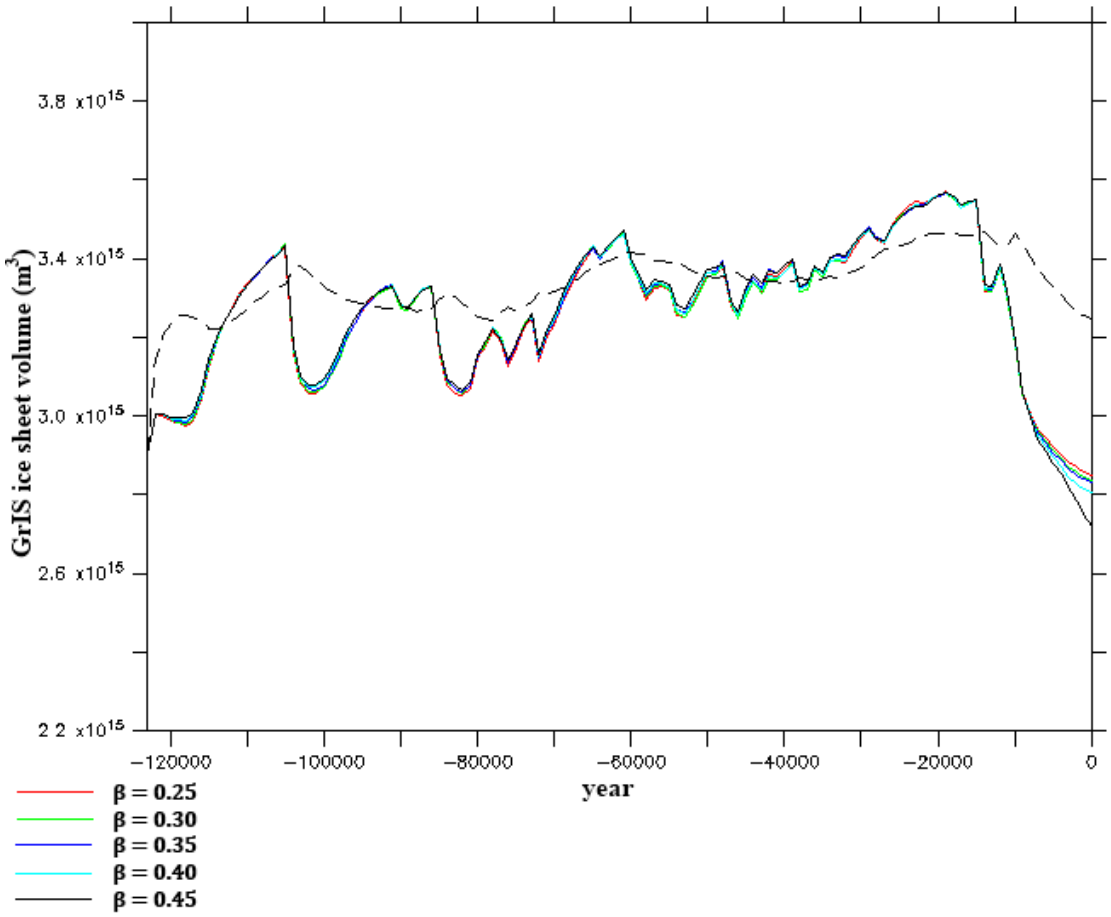


Figure 12: Time evolution of the GrIS ice sheet volume (in $m^3$) during the past-glacial period from 123 kyr b.p. up to 1850 ($t = 0$). The colored lines show results for different values of $\beta$. The black, dashed line shows the results obtained using the model of Helsen et al. (2012), started at the same time. The ice on Ellesmere Island is excluded from the total ice sheet volume.

which could dampen ice sheet growth during glacial periods.

### 4.3 Finding a value for $\beta$

In the previous sections, ice sheet growth has been modeled for different values of the $\beta$ parameter in the run-off parameterization of the SMB model used for this research. These experiments provided a general indication on suitable values of $\beta$, but a more precise estimate is needed. To accomplish this, the performance of the model should be measured against present-day observational values. Of course, not every aspect of the GrIS is closely constrained by measurements, as some variables are more difficult to acquire observational data of than others.

The variable used here to compare model results with is the total mass flux of the GrIS, which can also be expressed as the ice thickness change per year, $\frac{dH_i}{dt}$, integrated over the entire ice sheet. The observational estimate is taken from Shepherd et al. (2012), who used data from satellite altimetry, interferometry and gravimetry to estimate the total mass balance (see equation 18) for Greenland to be $-142 \pm 49$ Gt yr$^{-1}$ on average over the years 1992-2011. The optimal value for $\beta$ would then be the one whose model results show the closest approximation to this value, with its uncertainty range providing the upper and lower bounds for the choice of $\beta$, assuming that the temperature and precipitation fields from EC-Earth accurately represent present-day values.

Figure 13 shows the modeled total $\frac{dH_i}{dt}$ change over the GrIS for the period 1850-2100, which is the duration of the EC-Earth induced SMB forcing, for different values of $\beta$, ranging from 0.25 up to and including 0.45. Due to the use of yearly changing EC-Earth results as opposed to time-averaged data over a longer period, the data show a high degree of variability. However, a clear trend can be seen in the mass loss over the ice sheet during this period. Observations do not show a clear increase in mass loss over the GrIS until the mid-nineties. The model results seem to be in agreement with this: after 2000 the model results show a definite decrease of ice sheet mass. The resulting $\frac{dH_i}{dt}$ also becomes more variable, showing the dependency of temperature on run-off. Precipitation has also increased during this period, but the increase in temperature dominates over the increase in snowfall rates, leading to a decreasing ice sheet volume. This is in line with other studies (e.g. Graversen et al., 2011).

To finally assess which value for $\beta$ provides the highest agreement with present-day results, different values for $\beta$ have been plotted against the total $\frac{dH_i}{dt}$ over the ice sheet (as shown in figure 14, averaged over the period 1992-2011 (20 years), equal to the averaged result from Shepherd et al. (2012), which is plotted as the solid black line in the figure. The intersection between the observational value and the mass loss found for different values of $\beta$ provides the value which agrees most to present-day observations. From the figure, this value found is a $\beta$ of 0.41. The error in the measurements provides a lower bound of $\beta = 0.37$, and an upper bound of $\beta = 0.44$.

The graph also shows a nonlinear relation between $\beta$ and $\frac{dH_i}{dt}$. While seemingly linear for lower values of $\beta$, it appears to fall off more quickly as $\beta$ is further increased. Physically, this can be explained by reviewing that, following equation 15, if $\beta$ is increased, then the temperature-dependent run-off perturbation is increased compared to the reference field. The $H_s$ gradient increases, so a change in surface height will have a larger effect on the ablation. This leads to higher ablation for lower $\Delta H_s$ values. Consequently, not just the direct increase of $\beta$ counts towards a decrease

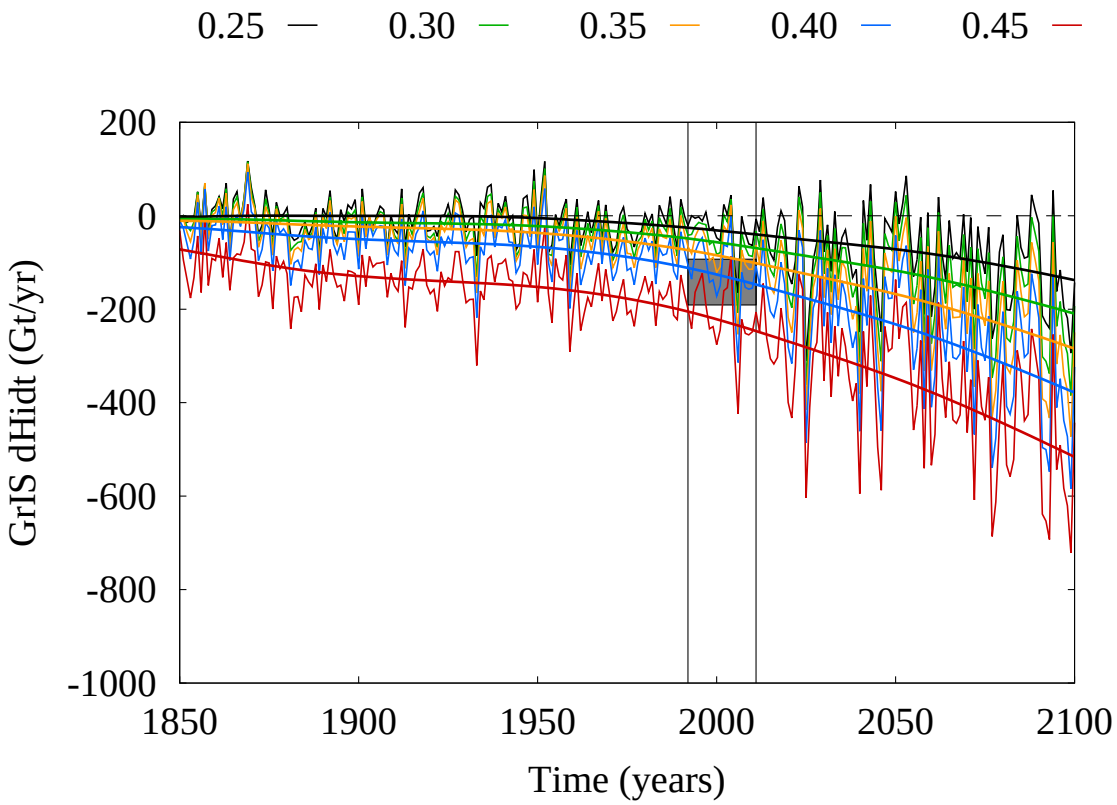


Figure 13: Total modeled $\frac{dH_i}{dt}$ over the GrIS from 1850 to 2100. Different colored lines indicate different values of $\beta$ (shown on top of the figure). Smoothed curves of the data are shown in thick lines. The vertical lines indicate the period 1992-2011, over which an average value was taken in order to determine $\beta$. The grey box shows the uncertainty range of the observational value for the 1992-2011 average taken from Shepherd et al. (2012).

of $\frac{dH_i}{dt}$, but a decrease of $\frac{dH_i}{dt}$ also provides feedback into the ablation parameterization as this lowers the surface height, leading to more ablation. This means that the relation between $\beta$ and $\frac{dH_i}{dt}$ is nonlinear.

## 4.4 Runs with optimal $\beta$

### 4.4.1 Past glacial forcing

Figure 15 shows the different contributions to the total mass flux per year for the spin-up period prior to the forcing with EC-Earth data. Here, it can be seen that the resulting $\frac{dH_i}{dt}$ is positive for large periods during the past glacial period, indicating ice sheet growth. Ablation frequently drops to zero during cold periods, which is expected, as temperatures were simply too low for surface melt to occur. Instead, the ice discharge over the edges of the ice sheet becomes the main source of mass loss during these periods: it behaves inversely to the ablation. The sharp peaks in the

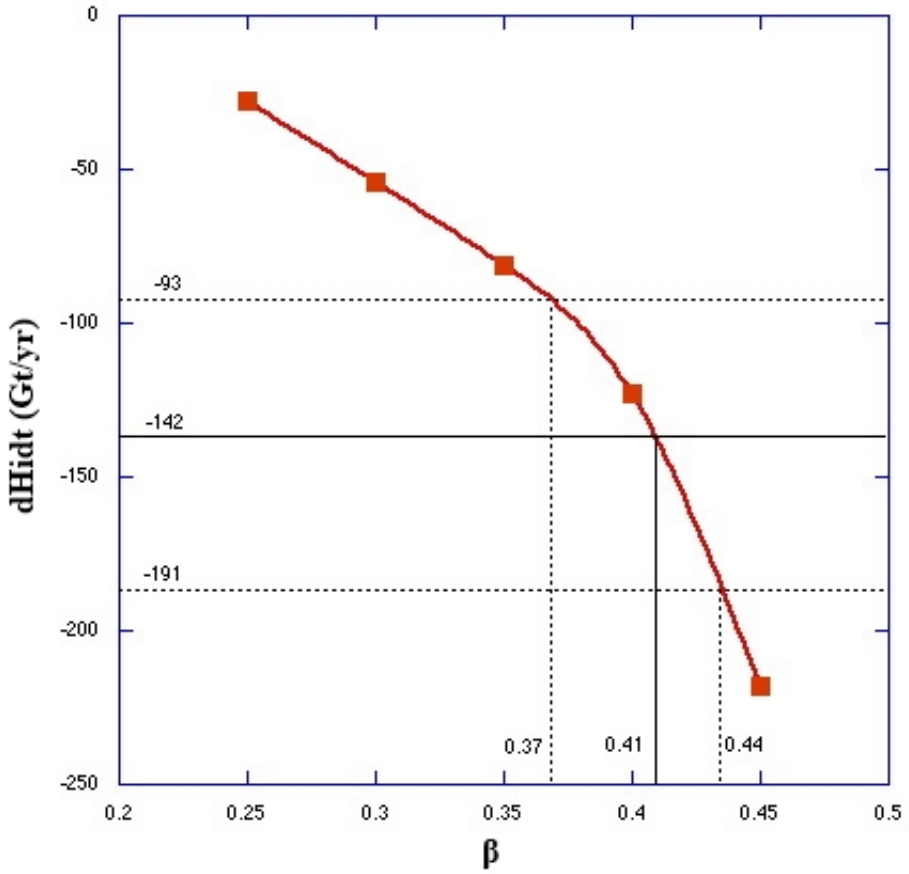


Figure 14: 1992-2011 average $\frac{dH_i}{dt}$ over the GrIS for different values of $\beta$. Results have been marked with red squares. The solid, horizontal black line indicates the observational result from Shepherd et al. (2012), with the dashed black lines showing the upper and lower margin of the uncertainty range. The intersection of the red line with the observational data gives the optimal result for the choice of $\beta$, with the intersections with the upper and lower errors providing an upper and lower bound for the value of $\beta$.

figure coincide with Dansgaard-Oeschger events, where sudden warming occurred for relatively short periods. In particular, two events between 80 and 70 kyr b.p. produced significant melt over the ice sheet. The transition into the present interglacial has the ice sheet lose a lot of its mass before settling around the balance point.

Accumulation does not vary as much as ablation over the course of this run, as the precipitation field itself is a constant throughout the spin-up period, only varying with the snow fraction and the temperature dependence within the parameterization.

### 4.4.2 1850 results

At the start of the forcing, in this case the year 1850, the ice sheet should be in balance, as 1850 is the reference year and thus the termperature offset $\Delta T$ becomes

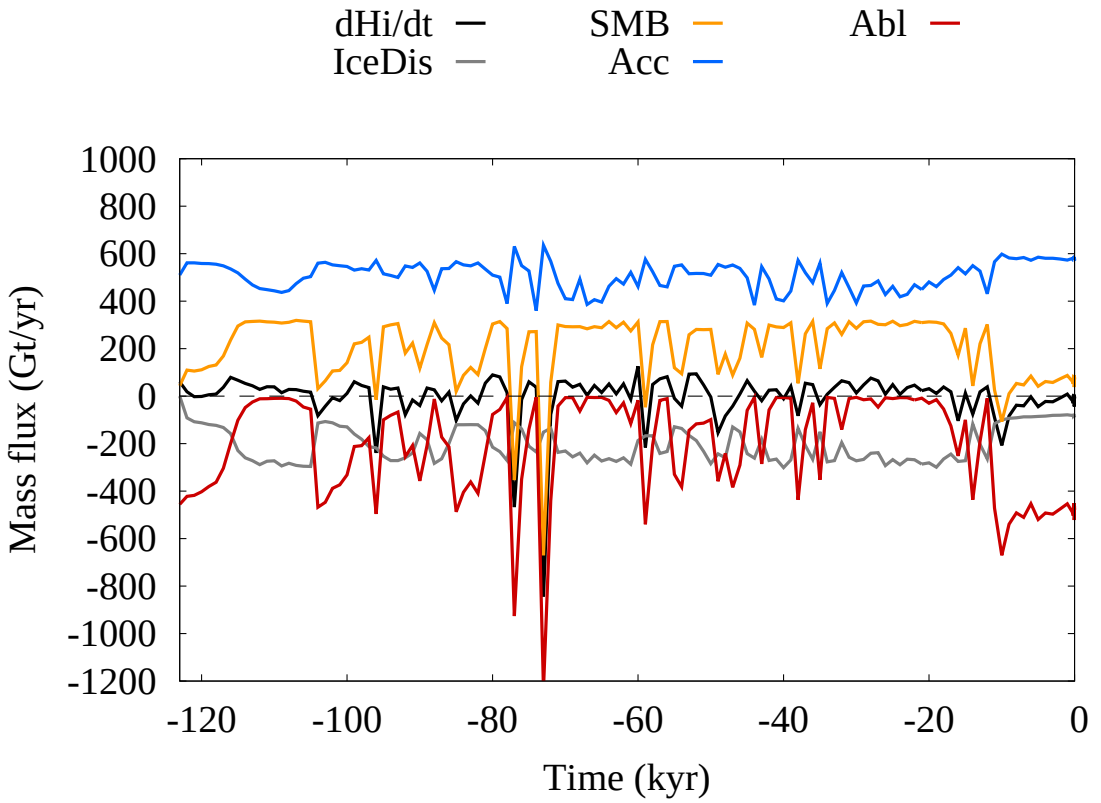


Figure 15: Different contributions to the total $\frac{dH_i}{dt}$ (in gigatons $\mathrm{yr}^{-1}$) for the past-glacial spin-up forcing. Accumulation (blue) and ablation (red) constitute the SMB (yellow). Ice discharge, $D$, is given in grey. The total $\frac{dH_i}{dt}$ over the ice sheet, indicated by the black line, is the net result of SMB and $D$.

zero. The resulting fields for $H_i$ and SMB at this time are shown in figure 16. It can be seen from the figures that the resulting ice sheet is in reasonable agreement with the observational values, with the main points of disagreement in the accumulation area at the southeast and the ablation area in the southwest. Especially in the latter section, the parameterization for the run-off overestimates the mass loss, as can also be seen when looking at the SMB values. The result is that at this point, the ice sheet has retracted somewhat compared to the observational values. Helsen et al. (2012) also reported an overestimation of mass loss in this area. In the ice sheet interior, the resulting values for ice thickness are generally lower than observational values. The low SMB in the accumulation in the southeast can be explained by the accumulation from the EC-Earth 1850 field being lower in both intensity and resolution compared to the accumulation from the RACMO2/GR regional climate model. The higher resolution provided by RACMO2/GR shows local peaks of precipitation (Ettema et al., 2009), which do not show from EC-Earth data (figure 2).

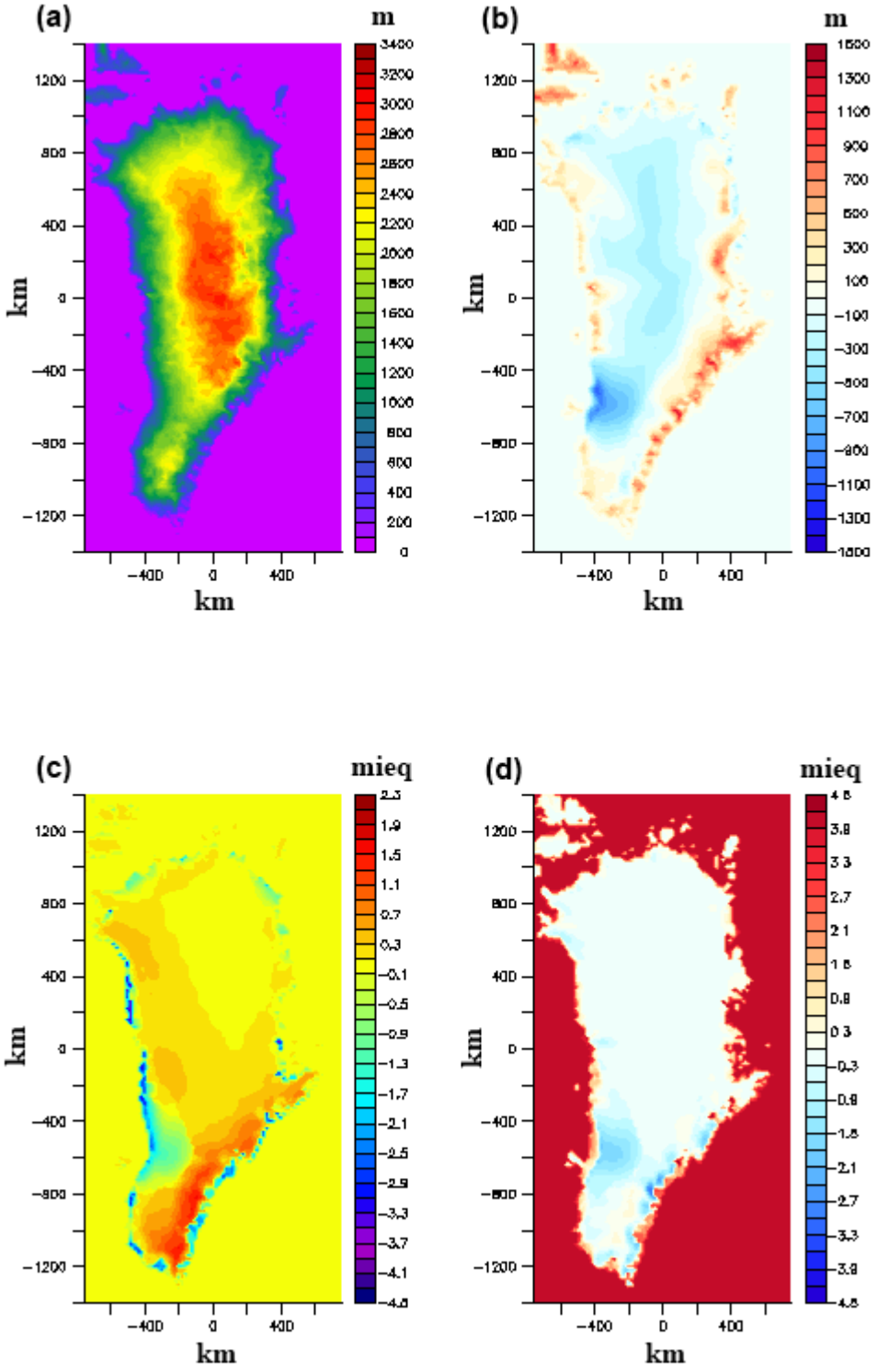


Figure 16: **(a)** Modeled ice sheet elevation (in metres a.s.l.) for 1850 and **(b)** difference with present-day observed elevation. **(c)** Surface mass balance (in m i.e.) for the GrIS for 1850. SMB is only calculated for ice sheet and grounding line points and is 0 otherwise to ensure mass conservation. **(d)** Difference of the 1850 mass balance with the 1958-2007 average SMB from the RACMO2/GR regional climate model. Note that the RACMO2/GR model prescribes an SMB value of -4 to points where ice is absent.

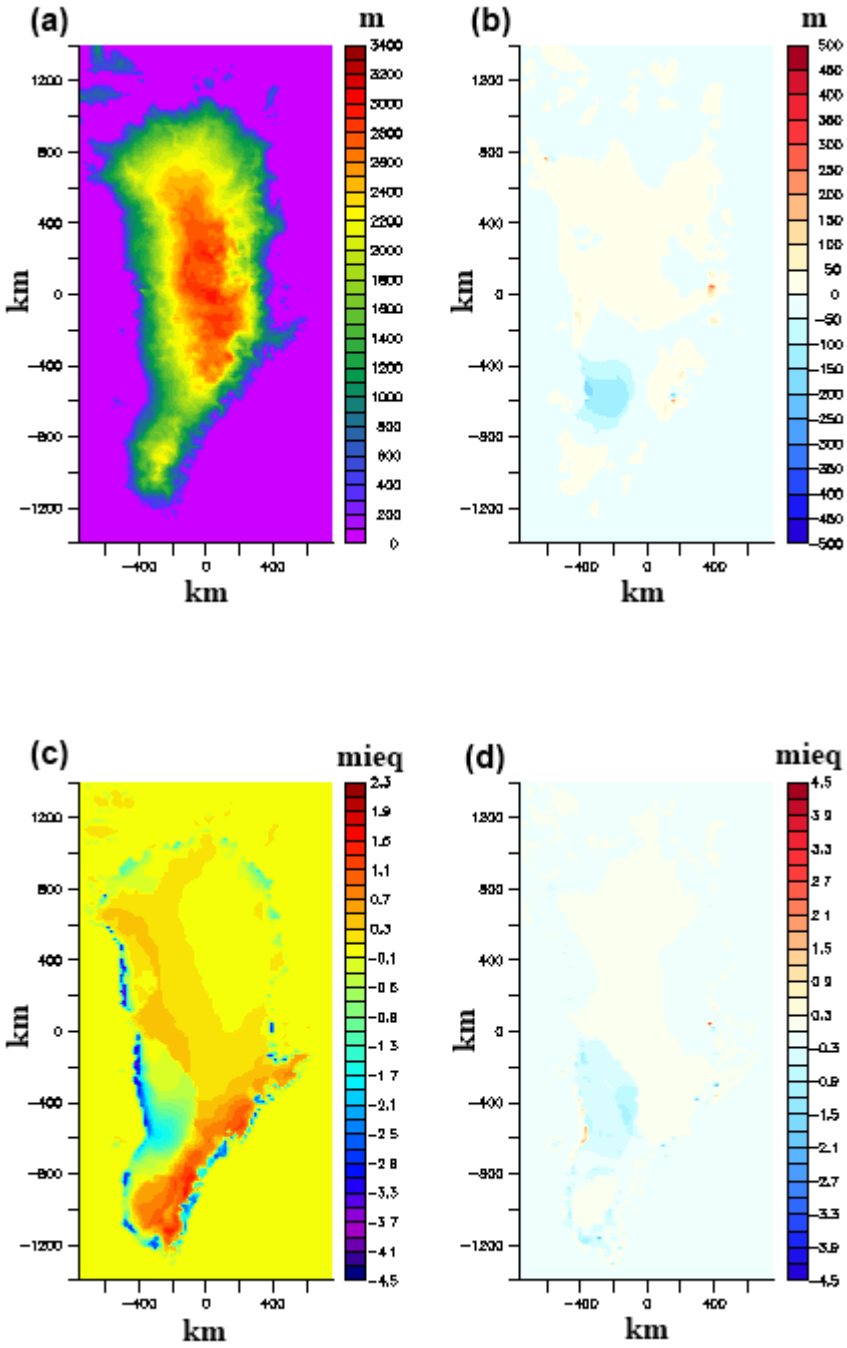


Figure 17: **(a)** Modeled ice sheet elevation (in metres a.s.l.) for 2000 and **(b)** difference with 1850. **(c)** SMB (in m i.e.) for the year 2000. SMB is only calculated for ice sheet and grounding line points and is 0 otherwise to ensure mass conservation. **(d)** Difference in SMB of between 2000 and 1850.

### 4.4.3 Present-day reconstruction

The results presented in figure 17a and c show the ice thickness and its SMB for the year 2000, which is after 150 years of EC-Earth climate forcing. This point in time is to most closely represent present-day results, as the EC-Earth output switches here from its historic reconstruction to the future estimation following the RCP4.5 scenario (section 3.4). Comparing these results with those for 1850 (figure 17b and d), these show a slightly more negative SMB in the southwestern section, spread out over a larger area. This result deviates from the observational data, as the mass balance should not be negative over such a large portion of the ice sheet. While much of this area should be part of the accumulation zone, the temperature dependent surface height, $H_{s,\Delta T}$, drops below the critical surface height due to increasing temperatures in these areas, allowing ablation over a larger area as more surface area moves from the accumulation zone into the ablation zone.

### 4.4.4 The K-transect

Examining the surface height gradient of the mass balance in the southwest ablation region provides a way of estimating the performance of the model in this region more closely. Observational data in this region is available for the IMAU K-transect. Along this transect line, located at 67° N, the IMAU has been measuring SMB for 21 years (Van de Wal et al., 2012) along several points from the base of the ice sheet up into the interior. The mean value of the measured SMB over these years provide a suitable comparison with the model data.

Figure 18 shows the model results and the observational data from van de Wal et al. (2012). In both cases, the 1990-2010 average is used. From these data, it can be seen that the mass balance gradient is lower than the observations, which can be attributed to a choice for $\beta < 1$. Moreover, the modeled SMB stays negative even at greater height, indicating that the ice sheet in this region is severely out of balance. Even for 1850, where the ablation should be close to the reference values (from RACMO2/GR), the SMB stays negative until a great height. Most likely, the low choice for $\beta$ lessens the SMB-$H_s$ gradient in the ablation area and thus lessens the ablation at low elevation, but overestimates the ablation at higher elevation. The gradient appears to level off at higher altitudes, which may be due to the $b_{\text{neg}}$ coefficient increasing in magnitude towards the interior of the ice sheet. As this coefficient was determined for calculating the net SMB rather than only using it to determine ablation (as was done for this project), this can possibly result in inaccuracies regarding the spatial variations in $b_{\text{neg}}$. However, Helsen et al. (2012) also predicted an overestimation of mass loss in this area.

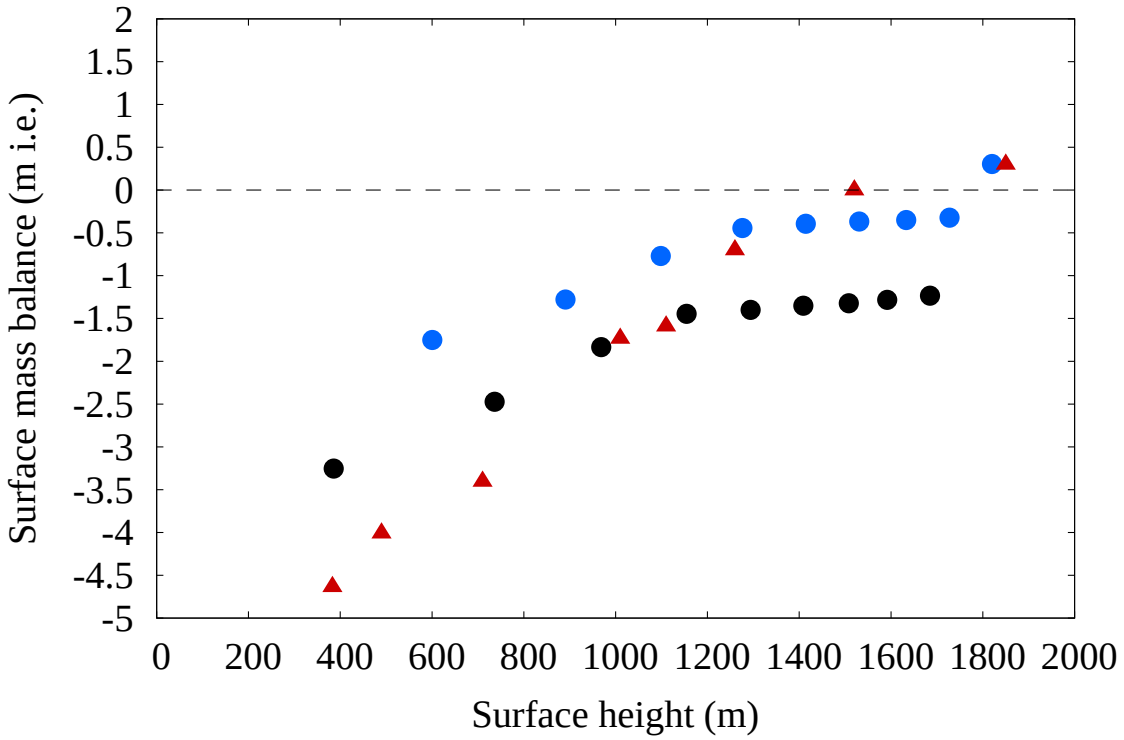


Figure 18: Surface mass balance as a function of elevation along the IMAU K-transect. The red triangles show the 1990-2010 twenty-one year average observational data from van de Wal et al. (2012). The modeled average over the same period is indicated with black dots. The blue dots represent the model results for the year 1850.

### 4.4.5 Future prediction

The $\frac{dH_i}{dt}$ values integrated over the ice sheet for $\beta = 0.41$, along with the lower and upper boundaries for the choice of this coefficient ($\beta = 0.37$ and $\beta = 0.44$, respectively), over the period 1850-2100 are shown in figure 19. The deviation of the lowest and highest possible choices for $\beta$ provide a measure for the uncertainty in the model for predicting the total mass loss of the Greenland Ice sheet. The mean loss for the ice sheet over the period 1850-2000 is 71.3 Gt yr$-1$ for the optimal $\beta$. For the low value of $\beta$, this is 40.8 Gt yr$-1$ and 134 Gt yr$-1$ for the highest estimate. For the period 2000-2100, the mean mass loss is 259 Gt yr$-1$, with the lowest estimate at 198 Gt yr$-1$ and the highest at 341 Gt yr$-1$.

The individual contributions to $\frac{dH_i}{dt}$ are presented in figure 20. The average SMB for the period 1958-2007 is -25.1 Gt yr$-1$, which is far from the result obtained by Ettema et al. (2009). They found a value of 469 $\pm$ 41 Gt yr$-1$ instead. Though they mention their findings to be larger than comparable recent model estimates due to the higher resolution of the accumulation field (section 4.4.2), the results obtained with this method show too low an SMB value.

The ice discharge $D$ appears to be more or less constant. This is most likely due to the absence of explicit calving physics and is instead calculated as the ice flow over the grounding line. The average ice discharge over the period 1958-2007 is -80 Gt yr−1, which is much less than observations show (Rignot et al., 2008). As both the SMB and $D$ are much lower than expected values, the resultant $\frac{dH_i}{dt}$ still appears to be within reasonable limits, though these values are generally also lower than other studies would suggest. The visible trend in $\frac{dH_i}{dt}$ up to 2100, however, does agree with other studies.

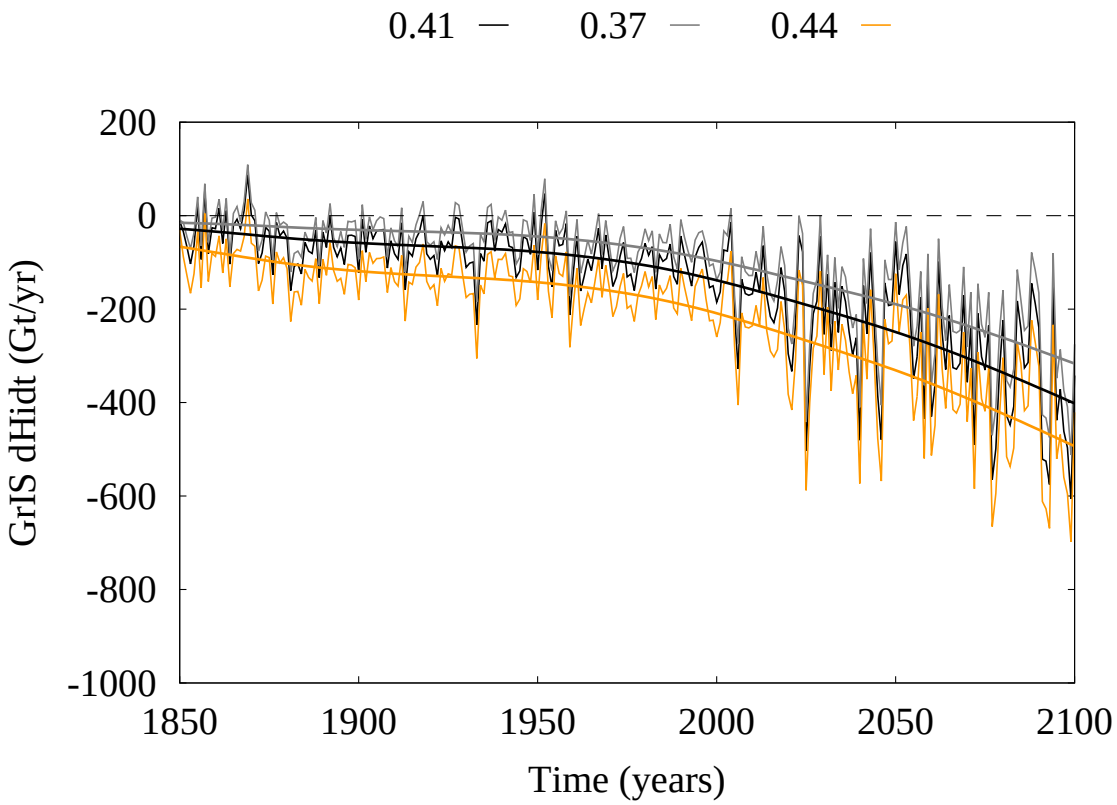


Figure 19: Total $\frac{dH_i}{dt}$ (in gigatons per year) for the GrIS over the period 1850-2100 for the optimal choice of $\beta$ (black), as well as the lower (grey) and upper (yellow) bounds for this choice. The thick curves are smoothed fits of the data lines.

The results for the ice thickness and the SMB at the end of the run are shown in figure 21. Especially the SMB shows the influence of the increase in temperature, leading to negative values over many parts of the ice sheet. While this was also the case for the present-day situation, it has become more widespread as well as more negative in the ablation zone. Near the K-transect, the SMB is most negative, which can be explained by the $b_{\text{neg}}$ coefficient (and thus the $H_s$-SMB gradient), which is relatively large in this area. This has led to a decrease in the ice sheet elevation (figure 21b) in this area and, consequently, a retraction of the ice sheet. For higher values of $\beta$, this area became even more pronounced. For the values on which the ice

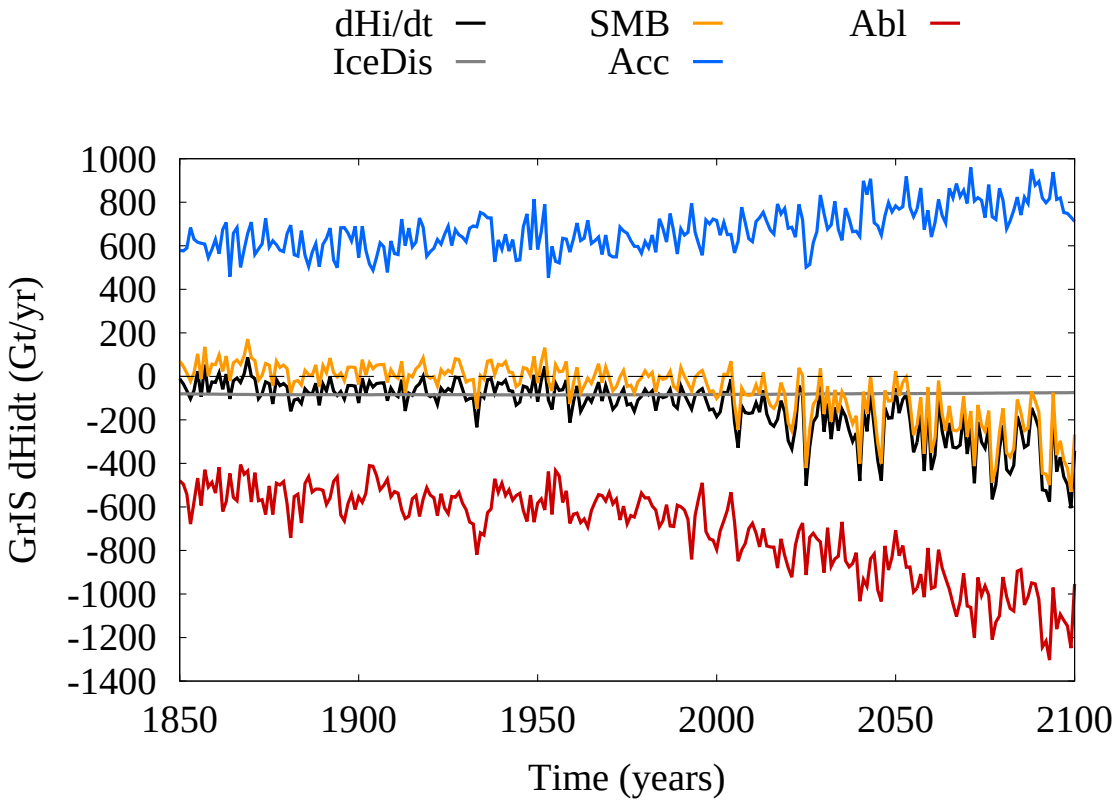


Figure 20: Different contributions to the total $\frac{dH_i}{dt}$ (black line) for the GrIS (in Gt yr$^{-1}$) over the period 1850-2100. SMB (yellow) is the net result of accumulation (blue) and ablation (red). SMB and the ice discharge, $D$, shown in grey, provide the net mass flux $\frac{dH_i}{dt}$ of the ice sheet.

sheet collapsed, this region provided the starting point, as here SMB values were the most negative. As the ice sheet is definitely out of balance at this point, continuing the run with values for $T$ and $P$ comparable to those predicted at 2100 could certainly cause the ice sheet to eventually collapse, but the model runs have not been extended past 2100 during this research.

The projected mass loss over the Greenland ice sheet can be translated into global sea-level rise. The results for model predictions for global sea-level rise are shown in figure 22. This figure shows a total contribution of melt over the GrIS to sea-level rise over the period 1850-2100 of 112 mm, with a range between 79 and 165 mm. Over the period 2000-2100, the model expects a sea-level rise of 79 mm, with the low $\beta$ predicting 61 mm and the high value 105 mm. This is well within the range of sea-level rise predicted by Graversen et al. (2011), who projects a range between 0 and 17 cm of sea-level rise, using the A1B and A2 greenhouse gas emission scenarios. For the period 1850-2000, the sea-level rise as calculated by the model may be overestimated due to the total mass flux during this period being too negative.

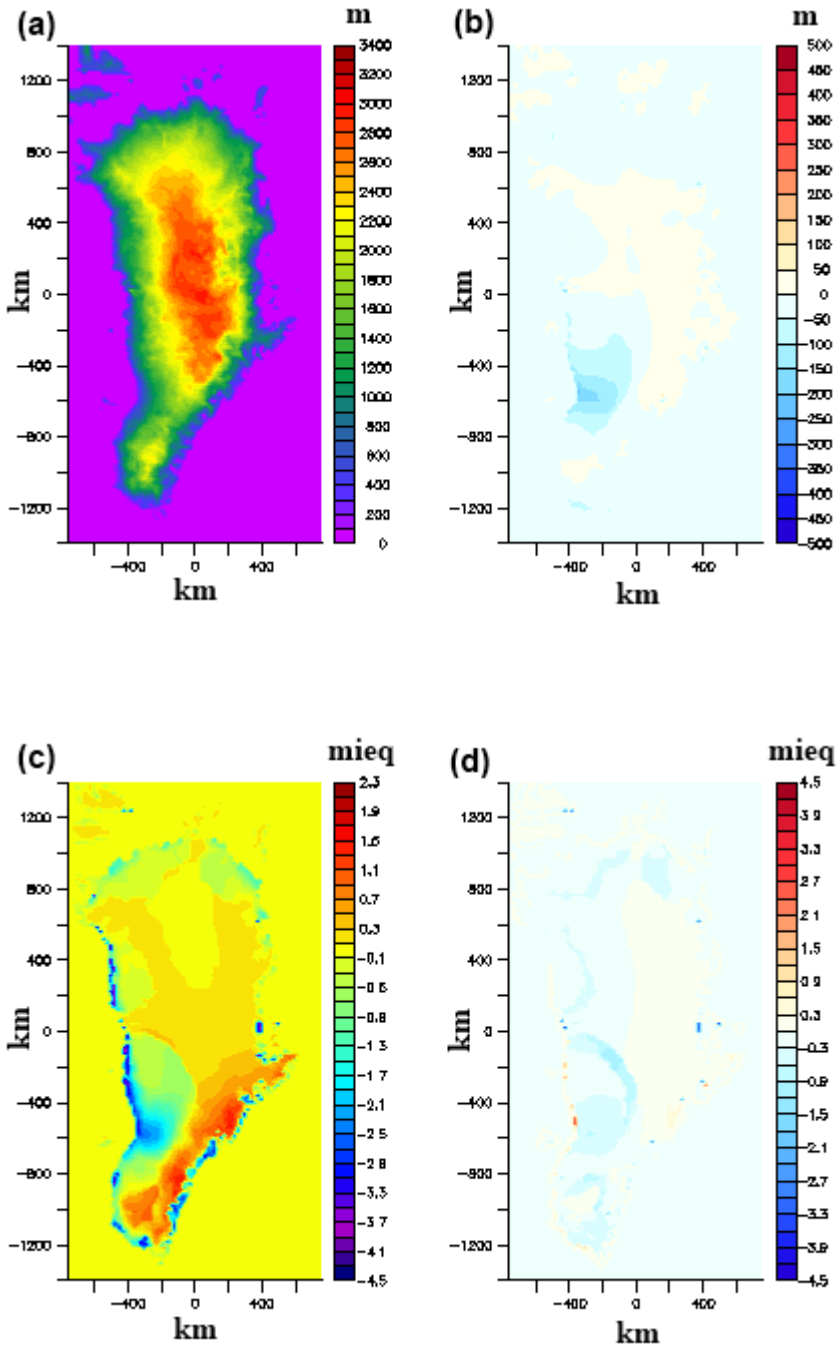


Figure 21: **(a)** Modeled ice sheet elevation (in metres a.s.l.) for 2100 and **(b)** difference with 2000. **(c)** Projected SMB (in m i.e.) for the year 2100. SMB is only calculated for ice sheet and grounding line points and is 0 otherwise to ensure mass conservation. **(d)** Difference in SMB between 2100 and 2000.

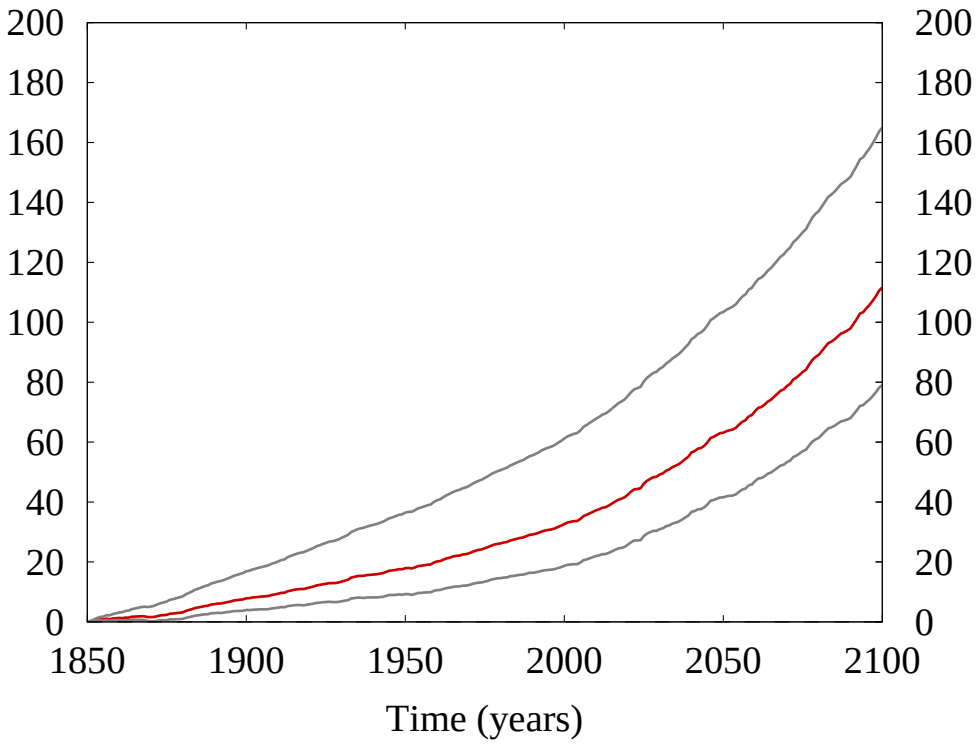


Figure 22: Projected sealevel rise (in mm) from 1850 to 2100. Results for $\beta = 0.41$ are shown in red. $\beta = 0.37$ and 0.44 are shown in grey, with the latter providing the upper bound estimate.

# Chapter 5
# Conclusion and discussion

Using EC-Earth output data in the forms of temperature and precipiatation fields to force the ice sheet model GRICE, projections have been made for the Greenland ice sheet over the course of the 21st century. A new method for calculating the run-off was introduced (a modified version of the SMB gradient method as presented by Helsen et al., 2012) in order to couple EC-Earth precipitation to the calculation of ice sheet SMB. Results for the 21st century are comparable to other works (e.g. Graversen et al., 2011) where sea-level rise is concerned, with the model predicting a sea-level rise over the period 2000-2100 between 61 and 105 mm.

Coupling EC-Earth data to the regional climate model GRICE led to difficulties mainly where the connection between the spin-up sequence and the forcing of SMB by EC-Earth data is concerned. In this project, the 1850 fields from EC-Earth were used as a reference value for forcing the spin-up track. However, runs without forcing show that the ablation had to be downscaled significantly in order for the ice sheet to find a balanced value by introducing a scaling parameter, $\beta$, to the parameterization for the ablation. This is probably caused by the precipitation from 1850 being lower in intensity than, for example, present-day values from Ettema et al. (2009). Downscaling the ablation especially led to a relatively poor representation of the SMB gradient along the K-transect, where SMB remained negative even far into the interior of the ice sheet while underestimating it along the margin.

Reconstruction of present-day values of the Greenland ice sheet were achieved to varying degrees of success. Ice sheet volume was slightly lower than observations (Bamber et al., 2003), but within reasonable values. SMB and the ice discharge, though, were both much lower than the values found by Ettema et al. (2009) and Rignot et al. (2008), respectively. However, the resulting value of the total mass flux of the GrIS was acceptable, though it remained negative even at times where the ice sheet should have been in balance or near balance.

In conclusion, the goals presented in section 1.4 have been achieved, though there still exists considerable room for improvement, especially where the parameterization of the ablation is concerned. Coupling EC-Earth data to the GRICE ice sheet model provided acceptable results for the evolution of the Greenland ice sheet over the 21st century. Future research may be concerned with finding a more suitable parameterization for the ablation and in finding a better reference state, so that present-day values for the Greenland ice sheet may be reconstructed to a better degree. Further future outlook is to eventually reach a two-way coupling of EC-Earth

and a model for the Greenland ice sheet by feeding calculations for surface height and albedo back to EC-Earth. This project, however, provides a first step towards achieving this goal.

## References

J. L. Bamber, D.J. Baldwin, and S. P. Gogineni. A new bedrock and surface elevation dataset for modelling the Greenland ice sheet. *Ann. Glaciol.*, 37(1):351–356, 2003.

R. Bindschadler. The importance of pressurized subglacial water in separation and sliding at the glacial bed. *J. Glaciol.*, 29:3–19, 1983.

R. Bintanja and R. S. W. van de Wal. North American ice-sheet dynamics and the onset of 100,000-year glacial cycles. *Nature*, 454:869–872, 2008.

R. Bintanja, R. S. W. van de Wal, and J. Oerlemans. Global ice volume variations through the last glacial cycle simulated by a 3-D ice-dynamical model. *Quat. Int.*, 95–96:11–23, 2002.

R. Bintanja, R. S. W. van de Wal, and J. Oerlemans. Modelled atmospheric temperatures and global sea levels over the past million years. *Nature*, 437:125–128, 2005.

B. de Boer, R. S. W. van de Wal, L. J. Lourens, R. Bintanja, and T. J. Reerink. A continuous simulation of global ice volume over the past 1 million years with 3-D ice-sheet models. *Clim. Dyn.*, 2012. doi: 10.1007/s00382-012-1562-2.

J. Ettema, M. R. van den Broeke, E. van Meijgaard, W. J. van de Berg, J. L. Bamber, J. E. Box, and R. C. Bales. Higher surface mass balance of the Greenland ice sheet revealed by high-resolution climate modeling. *Geophys. Res. Lett.*, 36:L12501, 2009. doi: 10.1029/2009GL038110.

R. G. Graversen, S. Drijfhout, W. Hazeleger, R. van de Wal, R. Bintanja, and M. Helsen. Greenland's contribution to global sea-level rise by the end of the 21st century. *Clim. Dyn.*, 37:1427–1442, 2011. doi: 10.1007/s00382-010-0918-8.

R. Greve. Relation of measured basal temperatures and the spatial distribution of the geothermal heat flux for the Greenland ice sheet. *Ann. Glaciol.*, 42:424–432, 2005.

M. M. Helsen, R. S. W. van de Wal, M. R. van den Broeke, W.J. van de Berg, and J. Oerlemans. Coupling of climate models and ice sheet models by surface mass balance gradients: application to the Greenland ice sheet. *The Cryosphere*, 6:255–272, 2012. doi: 10.5194/tc-6-255-2012.

K. Hutter. *Theoretical glaciology: material science of ice and the mechanics of glaciers and ice sheets*. Reidel Publ. Co., Dordrecht, 1983.

J. Jouzel and L. Merlivat. Deuterium and oxygen 18 in precipitation: modeling of the isotopic effects during snow formation. *J. Geophys. Res.*, 89:11749–11757, 1984.

E. Le Meur and P. Huybrechts. A comparison of different ways of dealing with isostasy: examples from modelling the Antarctic ice sheet during the last glacial cycle. *Ann. Glaciol.*, 23:309–317, 1996.

M. Meinshausen, S. J. Smith, K. Calvin, J. S. Daniel, Kainuma M. L. T., J-F. Lamarque, K. Matsumoto, S. A. Montzka, S. C. B. Raper, K. Riahi, A. Thomson, G. J. M. Velders, and D. P. P. van Vuuren. The RCP greenhouse gas concentrations and their extensions from 1765 to 2300. *Climate Change*, 109:213–241, 2011. doi: 10.1007/s10584-011-0156-z.

A. Ohmura, P. Calanca, M. Wild, and M. Anklin. Precipitation, accumulation and mass balance of the Greenland ice sheet. With 5 figures. *Zeitschrift fur Gletscherkunde und Glazialgeologie*, 35(1):1–20, 1999.

N. Reeh. Parameterization of melt rate and surface temperature on the Greenland ice sheet. *Polarforschung*, 59:113–128, 1991.

T. J. Reerink, M. A. Kliphuis, and R. S. W. van de Wal. Mapping technique of climate fields between GCMs and ice models. *Geosci. Model Dev.*, 3:13–41, 2010. doi: 10.5194/gmd-3-13-2010.

E. Rignot, J. E. Box, E. Burgess, and E. Hanna. Mass balance of the Greenland ice sheet from 1958 to 2007. *Geophys. Res. Lett.*, 35:L20502, 2008. doi: 10.1029/2008GL035417.

A. Shepherd, E. R. Ivins, A. Geruo, V. R. Barletta, M. J. Bentley, S. Bettadpur, K. H. Briggs, D. H. Bromwich, R. Forsberg, N. Galin, M. Horwath, S. Jacobs, I. Joughin, M. A. King, J. T. M. Lenaerts, J. Li, S. R. M. Ligtenberg, A. Luckman, S. B. Luthcke, M. McMillan, R. Meister, G. Milne, J. Mouginot, A. Muir, J. P. Nicolas, J. Paden, A. J. Payne, H. Pritchard, E. Rignot, H. Rott, L. S. Sørensen, T. A. Scambos, B. Scheuchi, E. J. O. Schrama, B. Smith, A. V. Sundal, J. H. van Angelen, W. J. van de Berg, M. R. van den Broeke, D. G. Vaughan, I. Velicogna, J. Wahr, P. L. Whitehouse, D. J. Wingham, D. Yi, D. Young, and H. J. Zwally. A reconciled estimate of ice-sheet mass balance. *Science*, 338(6111):1183–1189, 2012. doi: 10.1126/science.1228102.

R. S. W. van de Wal. The importance of thermodynamics for modeling the volume of the Greenland ice sheet. *J. Geophys. Res.*, 104(D4):3887–3898, 1999a.

R. S. W. van de Wal. Processes of buildup and retreat of the Greenland ice sheet. *J. Geophys. Res.*, 104(D4):3899–3906, 1999b.

R. S. W. van de Wal, W. Boot, C. J. P. P. Smeets, H. Snellen, M. R. van den Broeke, and J. Oerlemans. Twenty-one years of mass balance observations along the K-transect, West Greenland. *Earth Syst. Sci. Data*, 4:31–35, 2012. doi: 10.5194/essd-4-31-2012.

J. Weertman. The theory of glacial sliding. *J. Glaciol.*, 5:287–303, 1964.